



**HAL**  
open science

## On the Effect of Historical SST Patterns on Radiative Feedback

Timothy Andrews, Alejandro Bodas-Salcedo, Jonathan M. Gregory, Yue Dong, Kyle C. Armour, David Paynter, Pu Lin, Angshuman Modak, Thorsten Mauritsen, Jason N. S. Cole, et al.

► **To cite this version:**

Timothy Andrews, Alejandro Bodas-Salcedo, Jonathan M. Gregory, Yue Dong, Kyle C. Armour, et al.. On the Effect of Historical SST Patterns on Radiative Feedback. *Journal of Geophysical Research: Atmospheres*, 2022, 127 (18), pp.e2022JD036675. 10.1029/2022JD036675 . insu-03847095

**HAL Id: insu-03847095**

**<https://insu.hal.science/insu-03847095>**

Submitted on 17 Nov 2022

**HAL** is a multi-disciplinary open access archive for the deposit and dissemination of scientific research documents, whether they are published or not. The documents may come from teaching and research institutions in France or abroad, or from public or private research centers.

L'archive ouverte pluridisciplinaire **HAL**, est destinée au dépôt et à la diffusion de documents scientifiques de niveau recherche, publiés ou non, émanant des établissements d'enseignement et de recherche français ou étrangers, des laboratoires publics ou privés.

1                   **On the effect of historical SST patterns on radiative feedback**

2  
3                   **Timothy Andrews<sup>1</sup> and Alejandro Bodas-Salcedo**

4                   Met Office Hadley Centre, Exeter, UK.

5                   **Jonathan M. Gregory**

6                   Met Office Hadley Centre, Exeter, UK and National Centre for Atmospheric Science, University of  
7                   Reading, Reading, UK.

8                   **Yue Dong**

9                   Department of Atmospheric Sciences, University of Washington, Seattle, WA, USA.

10                  Now at Lamont-Doherty Earth Observatory, Columbia University, Palisades, NY, USA.

11                  **Kyle C. Armour**

12                  Department of Atmospheric Sciences, University of Washington, Seattle, WA, USA and School of  
13                  Oceanography, University of Washington, Seattle, WA, USA.

14                  **David Paynter**

15                  NOAA/Geophysical Fluid Dynamics Laboratory, Princeton University, Princeton, NJ, USA.

16                  **Pu Lin**

17                  Program in Atmospheric and Oceanic Sciences, Princeton University, Princeton, NJ, USA.

18                  **Angshuman Modak and Thorsten Mauritsen**

19                  University of Stockholm, Department of Meteorology, Stockholm, Sweden.

20                  **Jason N.S. Cole**

21                  Canadian Centre for Climate Modelling and Analysis, Environment and Climate Change Canada,  
22                  Victoria, BC, Canada.

23                  **Brian Medeiros**

24                  National Center for Atmospheric Research, Climate and Global Dynamics Laboratory, Boulder, CO,  
25                  USA.

26                  **James J. Benedict**

27                  Rosenstiel School of Marine and Atmospheric Science, University of Miami, Coral Gables, FL, USA.

28                  Now at Los Alamos National Laboratory, Los Alamos, NM, USA.

29                  **Hervé Douville and Romain Roehrig**

30                  CNRM, Université de Toulouse, Météo-France, CNRS, Toulouse, France.

<sup>1</sup> Correspondence to Timothy Andrews ([timothy.andrews@metoffice.gov.uk](mailto:timothy.andrews@metoffice.gov.uk))

31  
32  
33  
34  
35  
36  
37  
38  
39  
40  
41  
42  
43  
44  
45  
46  
47

**Tsuyoshi Koshiro and Hideaki Kawai**

Meteorological Research Institute, Japan Meteorological Agency, Tsukuba, Japan.

**Tomoo Ogura**

National Institute for Environmental Studies, Tsukuba, Japan.

**Jean-Louis Dufresne**

Laboratoire de Météorologie Dynamique/IPSL, CNRS, Sorbonne Université, École Normale Supérieure, PSL Research University, École Polytechnique, Paris, France.

**Richard P. Allan**

National Centre for Earth Observation, University of Reading, Reading, UK.

Department of Meteorology, University of Reading, Reading, UK.

**Chunlei Liu**

South China Sea Institute of Marine Meteorology, Guangdong Ocean University, Zhanjiang, China.

**Submitted to *Journal of Geophysical Research***

**21<sup>st</sup> February 2022**

48 **Abstract**

49 We investigate the dependence of radiative feedback on the pattern of sea-surface temperature  
50 (SST) change in fourteen Atmospheric General Circulation Models (AGCMs) forced with observed  
51 variations in SST and sea-ice over the historical record from 1871 to near-present. We find that over  
52 1871-1980, the Earth warmed with feedbacks largely consistent and strongly correlated with long-  
53 term climate sensitivity feedbacks (diagnosed from corresponding atmosphere-ocean GCM abrupt-  
54 4xCO<sub>2</sub> simulations). Post 1980 however, the Earth warmed with unusual trends in tropical Pacific  
55 SSTs (enhanced warming in the west, cooling in the east) that drove climate feedback to be  
56 uncorrelated with – and indicating much lower climate sensitivity than – that expected for long-term  
57 CO<sub>2</sub> increase. We show that these conclusions are not strongly dependent on the AMIP II SST dataset  
58 used to force the AGCMs, though the magnitude of feedback post 1980 is generally smaller in eight  
59 AGCMs forced with alternative HadISST1 SST boundary conditions. We quantify a ‘pattern effect’  
60 (defined as the difference between historical and long-term CO<sub>2</sub> feedback) equal to  $0.44 \pm 0.47$  [5-  
61 95%]  $\text{W m}^{-2} \text{K}^{-1}$  for the time-period 1871-2010, which increases by  $0.05 \pm 0.04 \text{ W m}^{-2} \text{K}^{-1}$  if calculated  
62 over 1871-2014. Assessed changes in the Earth’s historical energy budget are in agreement with the  
63 AGCM feedback estimates. Furthermore satellite observations of changes in top-of-atmosphere  
64 radiative fluxes since 1985 suggest that the pattern effect was particularly strong over recent  
65 decades, though this may be waning post 2014 due to a warming of the eastern Pacific.

## 66 1. Introduction

### 67 1.1. Background

68 A common starting point for quantifying the sensitivity of the Earth's climate to external  
69 perturbations is consideration of the global-mean energy budget,  $N = F + \lambda T$ , where  $N$  is the net  
70 downward radiative flux at the top-of-atmosphere (TOA) (units  $\text{W m}^{-2}$ ),  $F$  the effective radiative  
71 forcing (units  $\text{W m}^{-2}$ ),  $\lambda$  the climate feedback parameter (units  $\text{W m}^{-2} \text{K}^{-1}$ , a negative number in this  
72 paper, but the opposite convention is also used) and  $T$  the surface-air-temperature change (units K)  
73 relative to an unperturbed steady state in which  $N=F=0$ . Applied to non-steady states, such as the  
74 Earth's historical record (since the 1800s),  $\lambda$  is determined via either (i) differences (denoted by  $\Delta$ )  
75 between two climate states (often present-day and pre-industrial) according to  $\lambda = (\Delta N - \Delta F)/\Delta T$  (e.g.  
76 Gregory et al., 2002; Otto et al., 2013; Sherwood et al., 2020), or (ii) regression in the differential  
77 form  $\lambda = d(N - F)/dT$  if the timeseries of  $N$ ,  $F$  and  $T$  are known (Gregory et al. 2004; Gregory et al.  
78 2020).

79 Until recently it was often assumed that  $\lambda$  was - to a good approximation - a constant property of the  
80 climate system, such that feedbacks that applied over the historical record also applied to the  
81 Earth's long-term response, as quantified by the canonical equilibrium climate sensitivity (ECS, units  
82 K) to a forcing from a doubling of  $\text{CO}_2$  ( $F_{2x}$ ) over pre-industrial levels. Thus ECS was estimated directly  
83 from historical changes in  $N$ ,  $T$  and  $F$ , according to  $\text{ECS} = -F_{2x}/\lambda = -F_{2x} \Delta T / (\Delta N - \Delta F)$  (e.g. Gregory et  
84 al., 2002; Otto et al., 2013, amongst many others).

85 However, it is now recognised that  $\lambda$  varies in time since a forcing is applied and with the strength  
86 and/or type of that forcing (e.g. Senior and Mitchell, 2000; Hansen et al., 2005; Andrews et al. 2012;  
87 Armour et al., 2013; Geoffroy et al., 2013; Rose et al. 2014; Gregory et al. 2015; Andrews et al. 2015;  
88 Marvel et al. 2016; Rugenstein et al. 2016; Richardson et al., 2019; Dong et al. 2020; Bloch-Johnson  
89 et al., 2021; Rugenstein and Armour, 2021). Hence  $\lambda$  is an 'effective feedback parameter' that applies  
90 only to the climate change over which it was calculated. More specifically, over the historical record  
91  $\lambda$  is thought to be more stabilizing (more negative, climate sensitivity smaller) than might operate in  
92 the long-term future, and so  $\lambda$  estimated from historical climate change would understate ECS (e.g.  
93 Gregory and Andrews, 2016; Zhou et al., 2016; Armour, 2017; Proistosescu & Huybers, 2017;  
94 Andrews et al., 2018; Marvel et al., 2018; Silvers et al., 2018; Lewis and Curry, 2018; Gregory et al.  
95 2020; Sherwood et al. 2020; Dong et al. 2021).

96 The reason for the underestimate of long-term ECS is that climate feedbacks setting  $\lambda$ , such as cloud  
97 and lapse-rate changes, vary with the pattern of surface warming. Proxy reconstructions of past  
98 equilibrium climates and atmosphere-ocean general circulation model (AOGCM) simulations of long-  
99 term climate change show an 'ENSO-like' temperature pattern with strong temperature changes in  
100 the eastern Pacific as well as the Southern Ocean, whereas observed historical warming shows more  
101 pronounced warming in the western equatorial Pacific relative to the tropical mean and cooling in  
102 the eastern Pacific and Southern Ocean over recent decades (e.g. Collins et al., 2013; Li et al., 2013;  
103 Andrews et al., 2015; Gregory and Andrews, 2016; Zhou et al., 2016; Dong et al., 2019; Sherwood et  
104 al., 2020; Rugenstein et al. 2020; Olonscheck et al., 2020; Fueglistaler and Silvers, 2021; Watanabe et  
105 al. 2021; Power et al. 2021; Tierney et al. 2019; 2020).

106 Thus, more-stabilizing feedbacks have occurred over the historical record because enhanced  
107 warming in the western Pacific warm pool – a region of deep ascent and convection – results in a  
108 stronger negative lapse-rate feedback widely across the tropics due to efficient warming of the free  
109 troposphere, which in turn causes increased cloudiness (a negative cloud feedback) in the eastern

110 tropical Pacific due to remotely controlled increased lower tropospheric stability. In contrast, less-  
111 stabilizing feedbacks are expected in the future as enhanced warming in the eastern Pacific –  
112 characterised by descending air and marine low cloud decks which are capped under a temperature  
113 inversion and form over the relatively cool sea-surface-temperatures (SSTs) – results in a positive  
114 cloud feedback, without an accompanying negative lapse-rate feedback since the warming is  
115 ‘trapped’ in the boundary layer (e.g. Zhou et al., 2016, Andrews and Webb, 2018, Ceppi and Gregory,  
116 2017; Dong et al. 2019).

117 The dependence of radiative feedback on the pattern of surface temperature change has been  
118 termed a ‘pattern effect’ (Stevens et al., 2016), which distinguishes it from other feedback variations  
119 that might occur for example as a function of the magnitude of  $\Delta T$  (e.g. Block & Mauritsen, 2013;  
120 Caballero and Huber, 2013; Bloch-Johnson et al., 2021). Armour (2017) and Andrews et al. (2018)  
121 proposed a method to account for the pattern effect in estimates of ECS derived from historical  
122 climate changes via a modification of the energy budget approach. Their method requires an  
123 estimate of the difference in feedback,  $\Delta\lambda$ , due to the pattern effect between historical climate  
124 change and long-term ECS, so that  $ECS = -F_{2x}/(\lambda_{hist} + \Delta\lambda)$ , where  $\lambda_{hist}$  is the historical value. Since  $\Delta\lambda$  is  
125 found to be positive, it increases the best estimate of ECS and substantially lifts the upper  
126 uncertainty bound, but has only a small impact on the lower bound (Armour, 2017; Andrews et al.,  
127 2018; Sherwood et al. 2020).

128 One way of estimating the pattern effect,  $\Delta\lambda$ , is to contrast  $\lambda_{hist}$  in an Atmospheric GCM (AGCM)  
129 simulation forced by observed historical SST and sea-ice variations (termed an *amip-piForcing*  
130 simulation, see Section 2) with  $\lambda_{4xCO2}$  in the coupled AOGCM *abrupt-4xCO2* simulation with the same  
131 AGCM, so that  $\Delta\lambda = \lambda_{4xCO2} - \lambda_{hist}$  (Andrews et al. 2018). Note that here *abrupt-4xCO2* is being used as  
132 a surrogate<sup>2</sup> for long-term ECS. We assume other impacts on  $\lambda$ , such as the nature of the forcing  
133 agent – so called ‘efficacies’ (Hansen et al., 2005; Marvel et al. 2016; Richardson et al., 2019) –  
134 primarily occur due to forcing-specific impacts on historical SST patterns that will be included in the  
135 historical record, rather than any dependence on the actual forcing agent concentration in the  
136 atmosphere (which will be excluded in our design, because forcing levels are fixed at pre-industrial  
137 levels in *amip-piForcing*). On the other hand, *abrupt-4xCO2* experiments contain larger warming  
138 than the historical record, so any state dependence on  $T$  (e.g. Block & Mauritsen, 2013; Caballero  
139 and Huber, 2013; Bloch-Johnson et al., 2021) might erroneously be included in pattern effect  
140 estimates using this method.

141 The principal advantage of using *amip-piForcing* simulations in the calculation of the pattern effect is  
142 that  $\lambda_{hist}$  will be consistent with the SST patterns that occurred over the historical record. In contrast,  
143 one could use AOGCM historical simulations for  $\lambda_{hist}$ , but when AOGCMs are free to simulate their  
144 own historical SST patterns they struggle to reproduce the observed recent decadal trends in  
145 tropical Pacific SST patterns (Gregory et al. 2020; Fueglistaler and Silvers, 2021; Watanabe et al.  
146 2021; Dong et al., 2021) and the associated magnitude of  $\lambda_{hist}$ , thus underestimating the pattern  
147 effect (Gregory et al., 2020; Dong et al. 2021). This AOGCM bias in the pattern effect has important  
148 implications, which we return to in the Discussion, but our focus in this manuscript is on the

<sup>2</sup> We use  $\lambda_{4xCO2}$  rather than an equilibrium feedback,  $\lambda_{eqm}$ , because in practice equilibrium is difficult to achieve in AOGCMs due to the millennial timescales required to equilibrate the deep ocean. The feedback parameter associated with ECS is therefore often approximated from short ( $\sim 150$  years) *abrupt-4xCO2* experiments (Andrews et al. 2012). Technically this is still an ‘effective feedback parameter’ and associated ‘effective climate sensitivity’ (EffCS), but in practice it is found to provide a suitable analogue for long-term feedbacks in climate projections (Grose et al., 2018) and ECS (Sherwood et al. 2020) and so this distinction is not considered further (see Rugenstein et al. (2020) and Rugenstein and Armour (2021) for further discussion).

149 historical pattern effect as simulated by AGCMs *given* the observed SSTs, thus avoiding the issue of  
150 AOGCM biases in historical SST patterns. Note that while our focus is on the atmospheric response  
151 to a given SST pattern, causality can work in both directions. For example cloud feedback has been  
152 shown to have an impact on the pattern of tropical Pacific SST changes (Chalmers et al., 2022).

153 *amip-piForcing* simulations also show multi-decadal variations in  $\lambda_{\text{hist}}$  (Gregory and Andrews 2016;  
154 Zhou et al., 2016; Andrews et al., 2018; Fueglistaler and Silvers, 2021; Dong et al. 2021). In particular  
155  $\lambda_{\text{hist}}$  is generally most negative (pattern effect largest) over the most recent decades. This is because  
156 variations in atmospheric feedback are well explained by changes in SSTs in regions of tropical deep  
157 convection relative to the tropical-mean (Fueglistaler and Silvers, 2021) or global-mean (Dong et al.  
158 2019). Since the late 1970s, regions of deep convection have warmed by about +50% more than the  
159 tropical-mean (Fueglistaler and Silvers, 2021), and the eastern Pacific has cooled despite  
160 temperatures increasing globally (e.g. Hartmann et al. 2013; Power et al. 2021; and see our Figures 4  
161 and 9). Hence under this configuration of tropical Pacific SST change, we would expect negative  
162 feedback from the mechanisms described above (e.g. Zhou et al., 2016, Andrews and Webb, 2018,  
163 Ceppi and Gregory, 2017; Dong et al. 2019).

164 A limitation of the *amip-piForcing* experiment for quantifying  $\lambda_{\text{hist}}$  is that it may include a structural  
165 dependence on the underlying SST patterns and sea-ice in the Atmospheric Model Intercomparison  
166 Project (AMIP) II boundary condition data set (Gates et al., 1999; Hurrell et al., 2008; Taylor et al.,  
167 2000) used to force the *amip-piForcing* simulations (Andrews et al., 2018; Lewis and Mauritsen,  
168 2021; Zhou et al., 2021; Fueglistaler and Silvers, 2021). Different SST reconstructions have slightly  
169 different patterns of SST change over the historical period, and  $\lambda_{\text{hist}}$  may be affected. Indeed Lewis  
170 and Mauritsen (2021) and Fueglistaler and Silvers (2021) showed that warming in the tropical  
171 western Pacific relative to the tropical-mean is less pronounced in other SST datasets, and so we  
172 might expect less negative feedbacks ( $\Delta\lambda$  less positive) if the AGCMs were forced with non-AMIP II  
173 datasets.

174 Consistent with this expectation, Andrews et al. (2018) noted that in one AGCM the magnitude of  
175  $\lambda_{\text{hist}}$  was reduced by  $\sim 0.2 \text{ W m}^{-2} \text{ K}^{-1}$  when the AMIP II SSTs were replaced by HadISST2.1 SSTs (sea-ice  
176 remaining unchanged) in an *amip-piForcing* simulation. Partly because of this, Sherwood et al.  
177 (2020) and Forster et al. (2021) assessed the historical pattern effect to be smaller and more  
178 uncertain ( $\Delta\lambda = 0.5 \pm 0.5 \text{ W m}^{-2}$ ) than simply taking the *amip-piForcing* based model distribution  
179 reported by Andrews et al. (2018) ( $\Delta\lambda = 0.64 \pm 0.40 \text{ W m}^{-2}$ ). Subsequently, Lewis and Mauritsen  
180 (2021) and Zhou et al. (2021) also found  $\lambda_{\text{hist}}$  to be less negative ( $\Delta\lambda$  smaller) when using other SST  
181 datasets than AMIP II used in *amip-piForcing* simulations discussed here.

## 182 1.2. Aims and motivating questions

183 Andrews et al. (2018) provides much of the published quantitative analysis on  $\lambda_{\text{hist}}$  to observed SST  
184 patterns and  $\Delta\lambda$ , but only six AGCMs from only four different modelling centres were considered.  
185 Hence, a first motivation of this manuscript is to revisit their numbers with a broader set of models  
186 by utilizing the new *amip-piForcing* simulations from the Cloud Feedback Model Intercomparison  
187 Project phase 3 (CFMIP, Webb et al. 2017) contribution to the Coupled Model Intercomparison  
188 Project phase 6 (CMIP6, Eyring et al., 2016). The larger ensemble totalling 14 models when  
189 combined will provide a more robust quantification of the magnitude and spread of  $\lambda_{\text{hist}}$  and  $\Delta\lambda$  to a  
190 broader set of model physics and climate sensitivities (Zelinka et al. 2020; Meehl et al. 2020; Flynn  
191 and Mauritsen, 2020).

192 Secondly, the limited set of models in Andrews et al. (2018) prevented them from robustly exploring  
193 and quantifying the relationship between  $\lambda_{\text{hist}}$  and  $\lambda_{4\times\text{CO}_2}$  across models. In other words, it is not  
194 known whether feedbacks acting over the historical record in AGCMs are correlated to feedbacks  
195 acting on long-term ECS. For example is there a relationship between the two that could form the  
196 basis of an emergent constraint? Do different parts of the historical record relate better to  
197 feedbacks acting on long-term ECS than other parts, and why? As we will show, feedbacks over  
198 different parts of the historical record have different relationships to  $\lambda_{4\times\text{CO}_2}$ , and this is important for  
199 understanding what can and cannot be directly constrained from the historical record.

200 Thirdly,  $\lambda_{\text{hist}}$  and  $\Delta\lambda$  have been shown to vary substantially on decadal timescales with  $\lambda_{\text{hist}}$  being most  
201 negative (pattern effect largest) over recent decades since  $\sim 1980$  (Gregory and Andrews 2016; Zhou  
202 et al., 2016; Andrews et al., 2018; Gregory et al. 2020; Dong et al. 2021). This is consistent with the  
203 findings of Fueglistaler and Silvers (2021), who identified  $\sim 1980$  as the point in which the Earth  
204 begins to warm with a particular (even “*peculiar*”) configuration of tropical Pacific SSTs where  
205 “*regions of deep convection warm about +50% more than the tropical average*” driving large  
206 negative cloud feedbacks. Hence we are motivated to separate  $\lambda_{\text{hist}}$  and  $\Delta\lambda$  into a ‘before’ and ‘after’  
207 1980. This separation leads into our next motivating question.

208 Fourthly, are observations of recent decadal change since the 1980s consistent with the AGCMs? If  
209 so, what does a strong pattern effect in the presence of a substantial rate of global warming ( $\sim 0.19 \text{ K}$   
210  $\text{dec}^{-1}$ , Tokarska et al., 2020) imply for the efficiency of ocean heat uptake and is there any  
211 relationship between them? Loeb et al. (2020; 2021) identified a marked change in the Earth’s  
212 radiation budget post 2014 associated with the 2015/2016 El Niño event and a change in sign in the  
213 Pacific Decadal Oscillation (PDO) index. Such a shift in tropical Pacific SST patterns (a shift to  
214 warming in the eastern Pacific) should favour more positive feedbacks. We ask whether evidence of  
215 this is now potentially emerging in the satellite record.

216 Finally and fifthly, a limitation of the *amip-piForcing* approach, as discussed in Section 1.1, is that  $\lambda_{\text{hist}}$   
217 and  $\Delta\lambda$  derived from these experiments includes a structural dependence on the SST patterns and  
218 sea-ice in the AMIP II boundary condition data set used to force the AGCMs (Andrews et al., 2018;  
219 Lewis and Mauritsen, 2021; Zhou et al., 2021; Fueglistaler and Silvers, 2021). To investigate this  
220 further, we supplement the new *amip-piForcing* simulations with sensitivity tests with eight AGCMs  
221 forced with historical HadISST1 (Rayner et al., 2003) SSTs as per Lewis and Mauritsen (2021).

222 In summary, previous studies have shown that historical climate feedback ( $\lambda_{\text{hist}}$ ) varies on decadal  
223 timescales in *amip-piForcing* simulations and is larger in magnitude (climate sensitivity smaller) than  
224 that seen in long-term *abrupt-4xCO2* simulations associated with ECS, giving rise to a ‘pattern  
225 effect’. This is accentuated over recent decadal climate change. Here we make use of observations  
226 of the Earth’s energy budget from 1985 and a new suite of *amip-piForcing* simulations from  
227 CFMIP3/CMIP6 (giving us a combined ensemble of 14 models), as well as targeted HadISST1 versus  
228 AMIP II SST dataset sensitivity tests with eight AGCMs, to address the above question.

229 The manuscript is organised as follows: Section 2 describes the model and observational data.  
230 Section 3 presents the model results. Section 4 brings in the observational data. Section 5 presents a  
231 summary, discussion and outlook.

232

233

234



## 235 2. Methods and Data

### 236 2.1 *amip-piForcing*

237 To provide estimates of  $\lambda_{\text{hist}}$  consistent with the observed variations in SST patterns we turn to  
238 AGCMs forced with observed monthly variations in SSTs and sea-ice, while keeping all forcing agents  
239 such greenhouse gases and aerosols etc. constant at pre-industrial levels. Since the radiative forcing  
240 is constant ( $\Delta F=dF=0$ ) by construction,  $\lambda_{\text{hist}}$  can be diagnosed via  $\lambda_{\text{hist}} = dN/dT$  (or  $\Delta N/\Delta T$  if using finite  
241 differences between climate states) (Andrews, 2014; Gregory and Andrews, 2016, Zhou et al., 2016;  
242 Silvers et al., 2018; Andrews et al., 2018). Such an experimental design is now referred to as *amip-*  
243 *piForcing* (Gregory and Andrews, 2016). The experimental protocol builds on the Atmospheric Model  
244 Intercomparison Project (AMIP) design (Gates et al. 1999) that has long been used in climate  
245 modelling, but extends back to 1870 (rather than 1979 in AMIP) and forcing agents are kept at pre-  
246 industrial levels. As per AMIP, the underlying SST and sea-ice dataset used to force the AGCMs is the  
247 AMIP II boundary condition data set (Gates et al., 1999; Hurrell et al., 2008; Taylor et al., 2000). A  
248 description of the *amip-piForcing* protocol for CFMIP3/CMIP6 is given in Webb et al. (2017). When  
249 forced with observed monthly SSTs and sea-ice, AGCMs generally reproduce the observed  
250 relationships between surface temperature patterns, cloudiness and radiative fluxes well (Allan et  
251 al., 2014; Loeb et al. 2020), lending some credibility to the radiative effects of their simulated  
252 pattern effects to different SST patterns.

253 The *amip-piForcing* simulations used in this study are summarised in Table 1. They reflect a  
254 combination of new CFMIP3/CMIP6 simulations with the latest generation of models archived in the  
255 CMIP6 database and those used in Andrews et al. (2018) with some updates (see below). The  
256 exception is MPI-ESM1-2-LR (Mauritsen et al., 2019); this is a CMIP6 generation model but its *amip-*  
257 *piForcing* simulation is not currently included in the CMIP6 database. Note that this model contains  
258 the ECHAM6.3 atmospheric model, so the results ought to be very similar to the older ECHAM6.3  
259 simulations used in Andrews et al. (2018) and Lewis and Mauritsen (2021), though the models are  
260 not identical owing to differences in atmospheric composition and land surface properties (see  
261 Mauritsen et al., 2019, regarding the transition from MPI-ESM1.1 to MPI-ESM1.2). Furthermore, the  
262 newer MPI-ESM1-2-LR simulations include a longer time-period than the ECHAM6.3 simulations  
263 (Table 1).

264 The CFMIP3/CMIP6 *amip-piForcing* simulations begin in year 1870, but we discard the first year to  
265 be consistent with the earlier Andrews et al. (2018) ensemble which started in January 1871. The  
266 CFMIP3/CMIP6 simulations end in Dec 2014, whereas the simulations in the original Andrews et al.  
267 (2018) ensemble (largely) ended in Dec 2010. In part to address this, some of the Andrews et al.  
268 (2018) simulations have been rerun, including CAM4, GFDL-AM3 and GFDL-AM4 simulations, which  
269 now end in Dec 2014 or later (see Table 1). Another difference to Andrews et al. (2018) is that we  
270 now have an *abrupt-4xCO2* AOGCM simulation with GFDL-AM4 which they did not consider, to  
271 permit a quantification of the pattern effect in that model. In contrast, we exclude the Andrews et  
272 al. (2018) CAM5.3 simulation from our analysis since there is no *abrupt-4xCO2* AOGCM simulation to  
273 compare against.

274 The models used, time-periods covered and number of ensembles are detailed in Table 1. Where  
275 ensembles exist, an ensemble-mean  $dT$  and  $dN$  is created before analysis. Note that it makes little  
276 difference to  $\lambda$  if, alternatively, individual members are first analysed and then the results ensemble-  
277 meaned (Gregory and Andrews, 2016; Lewis and Mauritsen, 2021). All models share a common  
278 1871-2010 time-period and so the principal analysis is restricted to this time-period, but we consider  
279 the additional years to 2014 too. All data are global-annual-ensemble-means and expressed as

280 anomalies relative to an 1871-1900 baseline; the timeseries data has been made available (see Data  
281 Availability Section).

282 Unless otherwise stated all uncertainties in multi model ensemble-mean results represent a 5-95%  
283 confidence interval, calculated as  $1.645\sigma$  across models assuming a gaussian distribution. We do not  
284 attempt to adjust our uncertainty for the number of independent models,  $n$ , used in the ensemble  
285 (i.e. dividing by square root of  $n$ ). Our approach is similar to a "statistical indistinguishable ensemble"  
286 approach (Annan and Hargraves, 2011; 2017) though likely overstates the uncertainty in the true  
287 value if the ensemble shares characteristics of a "truth centred paradigm" (Sanderson and Knutti,  
288 2012).

## 289 2.2 HadSST-piForcing

290 To test the sensitivity of the *amip-piForcing* results to the underlying SST dataset, we repeat the  
291 *amip-piForcing* simulations with eight AGCMs (see Table 1) but replace the AMIP II boundary  
292 condition SST dataset with HadISST1 (Rayner et al. 2003). All other aspects of the simulations,  
293 including sea-ice, are identical to the *amip-piForcing* simulations. This is the same experimental  
294 design as Lewis and Mauritsen (2021), and we include their ECHAM6.3 simulations here (which again  
295 ought to be similar to the MPI-ESM1-2-LR simulations). The simulations cover a common time-period  
296 across models of 1871-2010, like in *amip-piForcing*, but some models are also extended further (see  
297 Table 1). We refer to these simulations as *hadSST-piForcing*, but note only the SSTs are from the  
298 HadISST1 dataset (hence 'hadSST' rather than 'hadISST'), the sea-ice remains as per *amip-piForcing*.  
299 Like *amip-piForcing*, all data are global-annual-ensemble-means and expressed as anomalies relative  
300 to an 1871-1900 baseline, and the timeseries data has been made available (see Data Availability  
301 Section).

302 Lewis and Mauritsen (2021) provide a summary of the source observational inputs used to construct  
303 the AMIP II and HadISST1 SST datasets and how they differ. In addition, we note that AMIP II uses  
304 HadISST1 SSTs (Rayner et al. 2003) prior to November 1981 and version 2 of the National Oceanic  
305 and Atmospheric Administration (NOAA) weekly optimum interpolation (OI.v2) SST analysis  
306 (Reynolds et al. 2002) thereafter. The merging procedure rebases the HadISST1 SSTs to avoid  
307 discontinuities in the merged dataset (Hurrell et al. 2008). Hence AMIP II and HadISST1 might be  
308 expected to be more similar before 1981, and diverge afterwards.

## 309 2.3 abrupt-4xCO2

310 A corresponding *abrupt-4xCO2* simulation using each AGCM's coupled AOGCM is used to determine  
311 the model's long-term sensitivity metrics ( $F_{4x}$ ,  $\lambda_{4xCO2}$  and  $ECS = -0.5 * F_{4x} / \lambda_{4xCO2}$ ) from regression of  
312 global-annual-mean  $dN$  against  $dT$  over 150 years of the simulations (see Andrews et al., 2012). We  
313 also use  $\lambda_{4xCO2}$  diagnosed from years 1-20 and years 21-150 of the *abrupt-4xCO2* simulation following  
314 Andrews et al. (2015), which approximately separates the two principal timescales of the climate  
315 response: the mixed-layer and deep-ocean (see Geoffroy et al. 2013 and Andrews et al. 2015).  
316 *abrupt-4xCO2 data* is available on the CMIP5 database (Taylor et al., 2012) for CCSM4, GFDL-CM3  
317 and HadGEM2-ES. All other abrupt-4xCO2 data is available on the CMIP6 database, except for  
318 HadCM3 and MPI-ESM1.1. For ECHAM6.3/MPI-ESM1.1, *abrupt-4xCO2* global-annual mean  $dN$  and  
319  $dT$  timeseries data are provided by Andrews et al. (2018). HadAM3 data is taken from Andrews et al.  
320 (2018) and Andrews et al. (2015); while a mean of seven realizations, this simulation is only 100  
321 years long so the calculations are over years 1-100 for  $\lambda_{4xCO2}$  and years 1-20 or 21-100 for the  
322 separation of timescales in this model.

323 Note when aligning each AGCM to its AOGCM, sometimes the AGCM and AOGCM model names  
324 differ in the literature. We indicate where this is applicable in Table 1. This does not apply to the  
325 newer CFMIP3/CMIP6 simulations which publish their AGCM and AOGCM simulations under  
326 consistent names.

#### 327 *2.4 Observations of recent decadal climate change*

328 To understand Earth's recent decadal climate change since ~1985 we turn to its observed global-  
329 mean energy budget (i.e.  $dT$ ,  $dN$  and  $dF$ ). For  $dT$  we use the HadCRUT5 analysis dataset (Morice et al.  
330 2021) (the current version is HadCRUT.5.0.1.0). This is an improvement on previous HadCRUT  
331 products and extends coverage in data sparse regions (see Morice et al. 2021). For  $dF$  we use the  
332 best estimate historical ERF timeseries produced by IPCC AR6 (Forster et al. 2021). For  $dN$  we use  
333 various versions of the DEEP-C satellite based reconstruction of the Earth's radiation balance from  
334 1985 to near-present. These are described in detail in Allan et al. (2014) and Liu et al. (2015; 2017;  
335 2020), but as we will use various versions of this product we give a brief overview here. The DEEP-C  
336 dataset is derived by merging satellite observations of top-of-atmosphere radiative flux timeseries  
337 from ERBE WFOV (Earth Radiation Budget Experiment Satellite wide field of view) and ECMWF  
338 reanalysis (ERA-Interim/ERA5) since 1985 with CERES (Clouds and the Earth's Radiant Energy  
339 System) satellite observed fluxes since March 2000. Hence prior to March 2000 it is largely informed  
340 by ERBE WFOV and ERA reanalysis, then aligns with CERES from March 2000. AMIP and high  
341 resolution AGCM simulations and reanalyses are used in the merging process to bridge the gaps  
342 between products and avoid discontinuities in the timeseries, including a gap in the satellite record  
343 during 1993 and 1999 (Allan et al. 2014). It is important to note that substantial uncertainty in  
344 decadal changes in  $dN$  associated with the merging process affects the record and this is  
345 conservatively estimated to be as high as  $0.5 \text{ Wm}^{-2}$  for changes applying across the whole record (Liu  
346 et al. 2020). However, uncertainty in the CERES period since March 2000 is much smaller based on  
347 assessment of instrument drift (Loeb et al. 2021). Various versions of the DEEP-C dataset exist which  
348 parallel updates to the underlying products and update the merging process. We use the latest  
349 version (DEEP-C v5, Liu and Allan 2022) for our principal analysis, which is based on CERES EBAF v4.1  
350 and ERBS WFOV v3, alongside ERA5 reanalysis and AMIP6 simulations (Liu and Allan, 2022). To  
351 illustrate structural uncertainties in our analysis we also use previous versions (v2, v3 and v4) of the  
352 DEEP-C datasets. The availability of datasets is provided in the Data Availability Section.  
353

#### 354 **3. Historical feedback and pattern effect in amip-piForcing and hadSST-piForcing simulations**

355 Figure 1a shows the multi-model ensemble mean  $dT$  timeseries in the *amip-piForcing* and *hadSST-*  
356 *piForcing* simulations, alongside an observed estimate from HadCRUT5 analysis dataset. The AGCM  
357 design reproduces the observed historical  $dT$  variability well (the correlation coefficient,  $r$ , between  
358 observed and both simulated  $dT$  timeseries is 0.97). However the AGCMs do not reproduce the  
359 observed trends precisely, notably omitting some observed warming in the most recent decades  
360 (Figure 1a; see also Andrews, 2014; Gregory and Andrews, 2016; Andrews et al. 2018). This is  
361 because in the AGCM design only the prescribed SSTs and sea-ice are evolving according to the  
362 observed dataset; the forcing agents (e.g. greenhouse gases, aerosols etc.) are prescribed at their  
363 preindustrial level and land temperatures are free to evolve. Hence the AGCMs are free to simulate  
364 their own land surface temperature variability (which may be different from that in the observed  
365 historical record) and trends, which are found to be smaller than that observed because the AGCMs  
366 do not include a land surface temperature change that arises as a consequence of increases in  
367 greenhouse gases and other forcing agents independent of SST changes (see Andrews, 2014;  
368 Gregory and Andrews, 2016; Andrews et al., 2018).

369 As  $dT$  increases,  $dN$  reduces (Figure 1b), i.e. the climate loses more heat to space as a consequence  
 370 of the climate response and feedbacks in the system. Figure 1c and 1d show the difference in the  $dT$   
 371 and  $dN$  timeseries between the *amip-piForcing* and *hadSST-piForcing* ensemble-mean response. For  
 372 most of the time the differences vary approximately about zero. However, larger differences are  
 373 evident from 1981 onwards, when the  $dN$  response in *amip-piForcing* is substantially larger than that  
 374 in *hadSST-piForcing* (Figure 1b and 1d), up to  $\sim 0.5 \text{ W m}^{-2}$  in some years (Figure 1d). This is consistent  
 375 with 1981 being the year in which the AMIP-II boundary condition source dataset switches from  
 376 HadISST1 to OI.v2 SST (see Section 3.2). This motivates us to separate the historical record into two  
 377 time-periods either side of 1980, i.e. 1871-1980 and 1981-2010 (Section 3.2).

378 However, we first consider feedback and the pattern effect that arises when calculated over the  
 379 historical record as a whole, rather than any time-period within (Section 3.1). This is useful for  
 380 informing studies that use the entire observed historical record to estimate ECS via energy budget  
 381 constraints (e.g. Andrews et al., 2018; Sherwood et al. 2020; Forster et al. 2021). It also allows a  
 382 direct comparison of our results using a broad ensemble of models to the narrower range of model  
 383 results reported by Andrews et al. (2018) and Lewis and Mauritsen (2021).

### 384 3.1 Considering the historical record as a whole

385 Figures 1e and 1f show the  $\lambda_{\text{hist}} = dN/dT$  relationship in the ensemble-mean *amip-piForcing* and  
 386 *hadSST-piForcing* simulation for 1871-2010.  $\lambda_{\text{hist}}$  is determined from ordinary least square linear  
 387 regression on global-annual-mean  $dN$  and  $dT$  timeseries data.  $\lambda_{\text{hist}}$  values for individual models are  
 388 given in Table 2 alongside their *abrupt-4xCO2* sensitivity metrics. Across the fourteen model  
 389 ensemble of *amip-piForcing* simulations  $\lambda_{\text{hist}} = -1.65 \pm 0.46 \text{ W m}^{-2} \text{ K}^{-1}$ , slightly smaller in magnitude  
 390 but with similar spread to the Andrews et al. (2018) ensemble (they reported  $\lambda_{\text{hist}} = -1.74 \pm 0.48 \text{ W m}^{-2} \text{ K}^{-1}$ ).  
 391 Like in Andrews et al. (2018), the spread in  $\lambda_{\text{hist}}$  is extremely similar to the spread in  $\lambda_{4xCO2}$  from  
 392 the coupled AOGCM *abrupt-4xCO2* ensemble (Table 2). The pattern effect,  $\Delta\lambda = \lambda_{4xCO2} - \lambda_{\text{hist}}$  between  
 393 *amip-piForcing* and *abrupt-4xCO2* (with  $\lambda_{4xCO2}$  from years 1-150 of *abrupt-4xCO2*) is  $\Delta\lambda = 0.70 \pm 0.47$   
 394  $\text{W m}^{-2} \text{ K}^{-1}$  across the ensemble (Table 3), which is slightly larger in magnitude but with more spread  
 395 than that reported by Andrews et al. (2018) ( $0.64 \pm 0.40 \text{ W m}^{-2} \text{ K}^{-1}$ ).

396 Tables 2 and 3 present the equivalent  $\lambda_{\text{hist}}$  and  $\Delta\lambda$  values when the AGCMs are forced with HadISST1  
 397 SSTs instead (*hadSST-piForcing*) and Figure 2 shows the relationship to *amip-piForcing*.  $\lambda_{\text{hist}} = -1.43 \pm$   
 398  $0.43 \text{ W m}^{-2} \text{ K}^{-1}$  in *hadSST-piForcing* (Table 2), which is smaller in magnitude but with similar spread to  
 399 the *amip-piForcing* results above. Subsetting to the eight AGCMs with both simulations,  $\lambda_{\text{hist}}$  is  $0.26 \pm$   
 400  $0.16 \text{ W m}^{-2} \text{ K}^{-1}$  smaller in magnitude in *hadSST-piForcing* but well correlated ( $r=0.94$ ) with *amip-*  
 401 *piForcing* values (Figure 2a, red points). The regression slopes of the red line in Figures 2a (slope =  
 402  $0.9 \pm 0.2$ ) and 2b (slope =  $1.1 \pm 0.4$ ) are statistically consistent with unity, implying there is little  
 403 AGCM dependence in the difference between  $\lambda_{\text{hist}}$  from *amip-piForcing* and *hadSST-piForcing*.  
 404 Hence, given the the strong correlation and close approximation of being parallel to the one-to-one  
 405 line (Figure 2, red points), we suggest a simple offset given by the difference ( $0.26 \pm 0.16 \text{ W m}^{-2} \text{ K}^{-1}$ )  
 406 well approximates the relationship between  $\lambda_{\text{hist}}$  over 1871-2010 in *amip-piForcing* and *hadSST-*  
 407 *piForcing*.

408 Despite  $\lambda_{\text{hist}}$  being smaller in magnitude in *hadSST-piForcing*,  $\Delta\lambda = 0.44 \pm 0.31 \text{ W m}^{-2} \text{ K}^{-1}$  is still large  
 409 and positive across the *hadSST-piForcing* ensemble (Table 3). The smaller uncertainty than the *amip-*  
 410 *piForcing* pattern effect likely reflects the narrower diversity of model physics in the smaller *hadSST-*  
 411 *piForcing* ensemble, for example we do not have *hadSST-piForcing* experiments for the models with  
 412 the largest (CESM2) or smallest (MIROC6) pattern effects in *amip-piForcing*. If we subset the *amip-*  
 413 *piForcing* ensemble to just those eight models with corresponding *hadSST-piForcing* experiments (Fig

414 2b, red points), then the spread (as measured by  $1.645\sigma$  in Table 3) across models in  $\Delta\lambda$  reduces  
415 from 0.47 to 0.28, which is similar to the spread found in *hadSST-piForcing*.

416 That a large pattern effect is present in the *hadSST-piForcing* simulation over the historical record is  
417 not in contradiction with the results of Lewis and Mauritsen 2021 (LM2021), who reported a  
418 ‘negligible unforced historical pattern effect’ with ECHAM6.3 when forced with HadISST1 SSTs. This is  
419 because LM2021 calculated their pattern effect by comparing  $\lambda$  from *hadSST-piForcing* to  $\lambda$  derived  
420 from a coupled AOGCM historical simulation, or approximations of it from years 1-70 of 1%CO<sub>2</sub> or  
421 years 1-50 of *abrupt-4xCO<sub>2</sub>* simulations. This necessarily gives a smaller pattern effect because it  
422 excludes many of the SST variations and patterns effects seen on longer timescales in CO<sub>2</sub> forced  
423 simulations (Senior and Mitchell, 2000; Gregory et al. 2004; Andrews et al. 2012; Armour et al.,  
424 2013; Geoffroy et al., 2013; Andrews et al. 2015; Rugenstein et al. 2016). While this might be useful  
425 for trying to quantify different mechanisms of the pattern effect (e.g. forced or unforced), it is a  
426 quantity we are less interested in, as we want to know the  $\lambda$  of relevance to long-term ECS and  
427 projections of the late 21<sup>st</sup> century. Therefore contrasting to  $\lambda_{4xCO_2}$  from years 1-150 is the most  
428 relevant metric (Sherwood et al., 2020), as we have done here.

429 Following Andrews et al. (2018) we decompose  $\lambda$  into its component longwave (LW) clear-sky,  
430 shortwave (SW) clear-sky and cloud radiative effect (CRE, equal to all-sky minus clear-sky fluxes)  
431 terms in Figure 3. Deviations away from the one-to-one line indicate a difference in *amip-piForcing*  
432 and *abrupt-4xCO<sub>2</sub>*  $\lambda$  (i.e. the pattern effect). Tables of the individual model results are given in the  
433 Supplementary Tables 1 - 3. It confirms the basic premise that historical LW clear-sky and cloud  
434 feedbacks are more stabilizing than under *abrupt-4xCO<sub>2</sub>*, consistent with the mechanistic and  
435 process understanding that the pattern effect arises predominantly from a lapse-rate (which affects  
436 LW clear-sky fluxes) and cloud feedback dependence on SST patterns (e.g. Zhou et al., 2016,  
437 Andrews and Webb, 2018, Ceppi and Gregory, 2017; Dong et al. 2019). Figure 3 also suggests there  
438 is a small compensation to the total pattern effect from SW clear-sky feedbacks, likely from sea-ice.  
439 That is, AGCMs forced with AMIP II boundary condition sea-ice changes have a slightly more positive  
440 feedback than found in their coupled *abrupt-4xCO<sub>2</sub>* simulations, though the difference is small  
441 (Figure 3). Consequently, a simple attribution of the difference in total feedback between *amip-*  
442 *piForcing* and *abrupt-4xCO<sub>2</sub>* to an SST driven pattern effect (as we have done here) will slightly  
443 understate the actual effect, though the term is small and we neglect it from now on. We discuss  
444 sea-ice uncertainties further below.

445 MIROC6 is the only model in the *amip-piForcing* ensemble to have near zero pattern effect (Table 3  
446 and note the single black dot on the one-to-one line in Figure 3). The reason for this different  
447 behaviour remains unclear. One could speculate that there is a relationship between a model’s  
448 climate sensitivity and its pattern effect, given that MIROC6 has the lowest ECS of all models  
449 consider here (ECS=2.6K, Table 2). However, we note that there is little correlation between ECS and  
450  $\Delta\lambda$  across models ( $r=0.4$ ) and that several other models with low ECS have large  $\Delta\lambda$ .

451 Alternatively, it could be that MIROC6’s atmospheric physics are largely insensitive to different SST  
452 patterns and/or that its AOGCM *abrupt-4xCO<sub>2</sub>* warming pattern is more similar to the historical  
453 record than other models. Both are potentially possible. For example,  $\lambda_{\text{hist}}$  for 1871-1980 and 1980-  
454 2010 separately (next Section and Table 2) shows that MIROC6 does simulate a pattern effect, but  
455 achieves a near zero pattern effect over the historical record as a whole by having a smaller (relative  
456 to other models) pattern effect over recent decades, offset by a negative pattern effect over the  
457 earlier period. In addition - and in contrast to other models - MIROC6 simulates a negative LW clear-  
458 sky pattern effect (red dot below the one-to-one line, Figure 3) which offsets its positive cloud  
459 feedback pattern effect.

460 The model with the largest pattern effect is CESM2 (Table 3). This occurs because of a particularly  
461 large cloud feedback sensitivity to SST patterns (grey dot furthest from the one-to-one line, Figure  
462 3). Zhu et al. (2022) argue that an issue in CESM2's cloud microphysics related to cloud ice number  
463 leads to an unrealistically large cloud sensitivity to warming in this model. Whether this is  
464 responsible for the model's large pattern effect is unclear. Mixed-phase clouds have not typically  
465 been associated with the pattern effect, though might clearly be of relevance to pattern effects over  
466 the Southern Ocean (Dong et al. 2020; Bjordal et al. 2020). It would be interesting in future work to  
467 identify the different cloud types associated with the pattern effect and sensitivity experiments with  
468 CESM2 to investigate which aspects of the cloud feedback change with different cloud microphysics  
469 schemes.

470 Many of our *amip-piForcing* (eleven models) and *hadSST-piForcing* (five models) simulations  
471 continue to Dec 2014 (Table 1), so we consider how this extended period affects the overall  
472 assessment of the historical pattern effect. In the eleven *amip-piForcing* simulations,  $\lambda_{\text{hist}} = -1.65 \pm$   
473  $0.48 \text{ W m}^{-2} \text{ K}^{-1}$  over 1871-2010, but this increases in magnitude to  $\lambda_{\text{hist}} = -1.71 \pm 0.51 \text{ W m}^{-2} \text{ K}^{-1}$  if  
474 calculated over 1871-2014 (Supplementary Table 4). An increase occurs in every model and the  
475 magnitude of change across the ensemble is  $0.07 \pm 0.06 \text{ W m}^{-2} \text{ K}^{-1}$  (Supplementary Table 4). In the  
476 five *hadSST-piForcing* simulations,  $\lambda_{\text{hist}} = -1.47 \pm 0.45 \text{ W m}^{-2} \text{ K}^{-1}$  over 1871-2010, but this increases in  
477 magnitude to  $\lambda_{\text{hist}} = -1.52 \pm 0.42 \text{ W m}^{-2} \text{ K}^{-1}$  if calculated over 1871-2014 (Supplementary Table 4). The  
478 magnitude of the increase ( $0.05 \pm 0.04 \text{ W m}^{-2} \text{ K}^{-1}$ ) is thus slightly smaller in this dataset  
479 (Supplementary Table 4).

480 While we have focused on the SST driven pattern effect, a remaining structural uncertainty in  
481 assessing total feedback differences between  $\lambda_{4\times\text{CO}_2}$  and  $\lambda_{\text{hist}}$  relates to the sea-ice dataset used to  
482 force the AGCMs. Andrews et al. (2018) provided a sensitivity test (see their Supplementary  
483 Material) by repeating the *amip-piForcing* simulation in two AGCMs but forced with HadISST2.1  
484 (Titchner and Rayner, 2014) SSTs and sea-ice. They found that the historical feedback parameter  
485 increased by  $\sim 0.6 \text{ W m}^{-2} \text{ K}^{-1}$  when forced with HadISST2.1 compared to AMIP II, and attributed most  
486 of this change to differences in the sea-ice datasets rather than SST. They noted that HadISST2.1 has  
487 substantially more pre-industrial Antarctic sea-ice concentration (see Titchner and Rayner, 2014),  
488 and so generated more sea-ice loss (more positive feedback) over the historical period (Andrews et  
489 al. 2018), as well containing large discontinuities in the timeseries. The historical sea-ice trends and  
490 associated feedbacks over the Southern Ocean in the HadISST2.1 dataset are difficult to reconcile  
491 with those found in AOGCMs and our physical understanding of them (Schneider et al. 2018). We do  
492 not pursue this further, but simply highlight that dataset assumptions made about pre-industrial sea-  
493 ice concentrations in Antarctica can have substantial impacts on diagnosed feedbacks in AGCMs and  
494 remains an outstanding uncertainty in assess total feedback differences. Fortunately, in *amip-*  
495 *piForcing* the difference in SW clear-sky feedback (which will be strongly impacted on by sea-ice  
496 feedbacks) is similar to that seen in  $\lambda_{4\times\text{CO}_2}$  (Figure 3) so this can be ignored if the focus is solely on SST  
497 driven feedbacks in the atmosphere.

498 In summary, for warming since the 1800s (using either 1871-2010 or 1871-2014), both *amip-*  
499 *piForcing* and *hadSST-piForcing* suggest a substantial pattern effect between radiative feedbacks  
500 operating over historical climate change and long-term ECS.

### 501 3.2 Considering the historical record before and after 1980

502 We now return the divergence in dN response between *amip-piForcing* and *hadSST-piForcing*  
503 simulations around 1980 (Figure 1d). As well as the change in behaviour discussed above, 1980  
504 provides a convenient separation of historical feedbacks and the pattern effect for two other

505 motivating reasons: (i) Fueglistaler and Silvers (2021) identify ~1980 as the point in which the Earth  
506 begins to warm with a particular configuration of tropical Pacific SSTs where regions of deep  
507 convection warm substantially more than the tropical mean, driving large negative cloud feedbacks  
508 and consistent with a large pattern effect over this period (Gregory and Andrews 2016; Zhou et al.,  
509 2016; Andrews et al., 2018; Gregory et al. 2020); and (ii) Fueglistaler and Silvers (2021) also identify  
510 ~1980 as a useful approximation of when the satellite era was integrated into the global observing  
511 system, and so developing an understanding of feedbacks and the pattern effect specifically from  
512 1980 onwards will aid interpretation of our most comprehensive observations of climate change and  
513 how they might relate to the future change (next Section).

514 Figure 4 compares the surface temperature trend over the two time-periods 1871-1980 and 1981-  
515 2010 in *amip-piForcing* and *hadSST-piForcing*. Differences between the two SST reconstructions are  
516 extremely subtle. For the earlier 1871-1980 time period, warming is more uniform, in part because  
517 of the longer time-period considered which will smooth out variability. Since 1981 in contrast, there  
518 has been strong western Pacific warming with eastern Pacific cooling, despite temperatures  
519 increasing in the global mean. Hence, we might expect a small pattern effect prior to 1980 and a  
520 large pattern effect post 1980 (e.g. Gregory and Andrews, 2016; Zhou et al., 2016, Andrews and  
521 Webb, 2018, Ceppi and Gregory, 2017; Dong et al. 2019, Fueglistaler and Silvers 2021).

522 Figures 1g and 1h show the  $\lambda_{\text{hist}} = dN/dT$  relationship in the ensemble-mean *amip-piForcing* and  
523 *hadSST-piForcing* simulation for 1871-1980 (grey points) and 1981-2010 (blue points). Results for  
524 individual models are given in Table 2. Figures 1g and 1h confirms the basic premise that  $\lambda_{\text{hist}}$   
525 strengthens in magnitude post 1980, consistent with the change in SST patterns (Figure 4).

526 For the earlier time-period, 1871-1980,  $\lambda_{\text{hist}} = -1.14 \pm 0.33 \text{ W m}^{-2} \text{ K}^{-1}$  in *amip-piForcing* is similar to  $\lambda_{\text{hist}}$   
527  $= -1.25 \pm 0.37 \text{ W m}^{-2} \text{ K}^{-1}$  in *hadSST-piForcing* (Table 2) – suggesting little sensitivity of the results to  
528 these two SST datasets over this time period. This is unsurprising given that the datasets are similar  
529 (though not identical) prior to this period (Section 2.2 and Figure 4). For the eight AGCMs that  
530 performed both simulations Figure 2a shows the relationship between  $\lambda_{\text{hist}}$  in *amip-piForcing* and  
531 *hadSST-piForcing*. For all time-periods  $\lambda_{\text{hist}}$  in *amip-piForcing* and *hadSST-piForcing* are found to be  
532 well correlated ( $r \geq 0.84$ , Figure 2a). For the earlier 1871-1980 results, the  $\lambda_{\text{hist}}$  values fall close to the  
533 one-to-one line (blue dots, Figure 2) and within the range of  $\lambda_{4\times\text{CO}_2}$  (grey shaded areas in Figure 2).  
534 This suggests that for 1871-1980  $\lambda_{\text{hist}}$  is broadly independent of the two SST datasets (consistent with  
535 their common basis) and that the pattern effect is small for this time period. Indeed, the 1871-1980  
536 pattern effect is small but positive ( $\Delta\lambda = 0.19 \pm 0.35 \text{ W m}^{-2} \text{ K}^{-1}$  in *amip-piForcing* and  $0.26 \pm 0.28 \text{ W m}^{-2}$   
537  $\text{K}^{-1}$  in *hadSST-piForcing*, Table 3 and Figure 2b).

538 In contrast, for 1981 onwards (i.e. 1981-2010),  $\lambda_{\text{hist}}$  is generally far from the  $\lambda_{4\times\text{CO}_2}$  range (i.e. a large  
539 pattern effect) and away from the one-to-one line (i.e. a dependence on the SST dataset) (Figure 2a;  
540 grey points). Indeed,  $\lambda_{\text{hist}}$  over 1981-2010 is substantially stronger in magnitude than over 1871-1980  
541 ( $\lambda_{\text{hist}} = -2.33 \pm 0.72 \text{ W m}^{-2} \text{ K}^{-1}$  in *amip-piForcing* over 1981-2010, Table 2; Figure 2a) and the pattern  
542 effect is large ( $\Delta\lambda = 1.38 \pm 0.75 \text{ W m}^{-2} \text{ K}^{-1}$ , Table 3; Figure 2b), although somewhat weaker in  
543 magnitude in *hadSST-piForcing* ( $\Delta\lambda = 1.12 \pm 0.69 \text{ W m}^{-2} \text{ K}^{-1}$ , Table 3; Figure 2b). For 1981-2010,  $\lambda_{\text{hist}}$  is  
544 generally weaker in *hadSST-piForcing* (Table 2; Figure 3a) by  $0.26 \pm 0.48 \text{ W m}^{-2} \text{ K}^{-1}$  across the eight  
545 AGCMs using both SST datasets.

546 These results are generally consistent with Fueglistaler and Silvers (2021) and Lewis and Mauritsen  
547 (2021) who both point to the AMIP II SST dataset as having larger (relative) western tropical Pacific  
548 warming than in other SST datasets, and hence from the process understanding we would expect a  
549 more negative feedback (and larger pattern effect) in *amip-piForcing*, as found above. The one

550 exception is GFDL-AM4, which simulates a more negative  $\lambda_{\text{hist}}$  under HadISST1 SSTs than AMIP II  
551 from 1981-2010, and so a larger pattern-effect over this period under HadISST1 SSTs (Tables 2 and 3  
552 and the single grey dots in Figures 2a and 2b which sit on the other side of the one-to-one line from  
553 the other models). The reasons for this remain unclear.

554 In summary we have shown that a division around 1980 usefully separates historical climate change  
555 into two time-periods: (i) pre 1981 the Earth warmed over most of the historical record with an  
556 averaged warming pattern that is relatively uniform, and feedbacks largely consistent with long-term  
557 ECS feedbacks (i.e. a relatively small pattern effect), and (ii) post 1980 where the Earth warmed with  
558 a particular configuration of strong SST gradients that drove feedbacks much more stabilizing than  
559 those seen in long-term ECS feedbacks (i.e. large pattern effect), albeit with a sensitivity of the  
560 magnitude of this result to the SST dataset considered.

### 561 *3.3 Relationships between historical and ECS feedbacks*

562 We now consider whether feedbacks over the historical period in *amip-piForcing* are related to  
563  $\lambda_{4\times\text{CO}_2}$ . This is in contrast to the previous sections which only quantified their difference (i.e. the  
564 pattern effect).

565 Firstly, we note that the spread in feedbacks across models over the earlier (1871-1980) time-period  
566 in *amip-piForcing* are well correlated with the spread in feedbacks across models in *abrupt-4xCO2*.  
567 ( $r=0.69$ , Figure 5a). In contrast, feedbacks over the most recent decades (1981-2010) are only weakly  
568 correlated with  $\lambda_{4\times\text{CO}_2}$  ( $r=0.27$ ). Secondly, feedback over the full historical record (1871-2010) is only  
569 weakly correlated with feedback from the 1871-1980 time-period ( $r=0.45$ , Figure 5b). In contrast,  
570 1871-2010 feedback is strongly correlated with feedback over the most recent 1980-2010 decades  
571 ( $r=0.91$ , Figure 4b). This strong correlation between 1981-2010 and the 1871-2010 feedback arises  
572 because the spread for 1871-2010 is dominated by the spread for 1981-2010.

573 Given that the feedbacks applying in 1871-1980 and in 1981-2010 are different, we infer that  
574 variation in the pattern of SST over these two periods is dominated by different effects. Because the  
575 feedbacks of 1871-1980 are correlated with *abrupt-4xCO2*, the difference between the two periods  
576 could be explained by CO<sub>2</sub> being the dominant influence in 1871-1980 SST patterns, while something  
577 else (e.g. perhaps variability, aerosol, volcanism) dominates during 1981-2010. This is only a  
578 hypothesis, because these experiments do not provide a way to attribute the observed SST changes  
579 to causes.

580 The result is that the spread in feedbacks over the full historical record are only weakly correlated  
581 with  $\lambda_{4\times\text{CO}_2}$  ( $r=0.51$ , Figure 3), because of the strong pattern effect post 1980. Hence, we can say little  
582 about future  $\lambda_{4\times\text{CO}_2}$  directly from climate change post 1980 or even the full historical record without  
583 adjusting for a pattern effect. In contrast, the feedbacks operating over the earlier 1871-1980 time-  
584 period are correlated with  $\lambda_{4\times\text{CO}_2}$  ( $r=0.69$ , Figure 5a), but here the climate change signal is smaller and  
585 the observations poorer which limits the utility of this time-period to act as an observational  
586 constraint.

587 That recent decadal feedbacks are the most unrepresentative of the long-term climate sensitivity is  
588 unfortunate, not just because it coincides with the advent of the satellite record and so is extremely  
589 well observed, but also because climate change since ~1980 ought to provide the best constraint on  
590 ECS (e.g. Jiménez-de-la-Cuesta and Mauritsen, 2019). This is because it offers a strong global  
591 warming signal, which AOGCMs attribute to greenhouse gas increases, while avoiding the  
592 uncertainty due to aerosol radiative forcing, which has only changed slowly over this period (at least  
593 globally, strong regional changes may have impacted on SST patterns, e.g. Smith et al. 2015;



594 Takahashi & Watanabe, 2016; Moseid et al., 2020). Although feedbacks operating over the earlier  
595 1871-1980 part of the historical record are correlated with long-term CO<sub>2</sub> induced feedbacks, a  
596 reliable observational constraint is harder because the climate change signal is smaller and the  
597 observations poorer. We discuss this further in the Discussion section.

598 Up to now we have only considered a comparison of *amip-piForcing* feedbacks to a single definition  
599 of *abrupt-4xCO2* feedbacks (i.e. feedbacks diagnosed over years 1-150 in *abrupt-4xCO2*). Here we  
600 briefly consider separating  $\lambda_{4xCO_2}$  into the two principal timescales of the *abrupt-4xCO2* response  
601 following Andrews et al. (2015) by calculating  $\lambda_{4xCO_2}$  over years 1-20 (a fast timescale) and 21-150 (a  
602 slow timescale) (Table 2). The rationale is that 20 years is approximately the timescale required for  
603 the mixed-layer to equilibrate in response to step forcing, and any subsequent climate response  
604 scaling with the slower deep-ocean timescale, as approximated by two-layer models (Held et al.,  
605 2010; Geoffroy et al., 2013; Gregory et al., 2015).

606 Figure 5c shows  $\lambda_{hist}$  from 1871-1980 is largely scattered about the one-to-one line with  $\lambda_{4xCO_2}$  from  
607 years 1-20, suggesting little to no pattern effect between these two. This is potentially consistent  
608 with the historical record largely being the result of the faster timescale responses (Held et al. 2010;  
609 Proistosescu & Huybers, 2017). In contrast, post-1980  $\lambda_{hist}$  is far from the one-to-one line (i.e. large  
610 pattern effect to years 1-20 of *abrupt-4xCO2*, Figure 5c) but is marginally correlated ( $r=0.53$ ),  
611 suggesting recent decades do contain some information relevant to the feedback seen in the fast  
612 timescale response to CO<sub>2</sub>. However, the longer-term feedbacks associated with the slow timescale  
613 response to CO<sub>2</sub> (years 21-150 of *abrupt-4xCO2*, Figure 5d) have no correlation with  $\lambda_{hist}$  post-1980  
614 ( $r=-0.06$ , Figure 5d). This is not surprising given that the eastern tropical Pacific and Southern Ocean  
615 have largely cooled in the post-1980 period, while they warm substantially over years 21-150 of  
616 *abrupt-4xCO2*.

### 617 618 3.4 Decadal variability in feedbacks and the pattern effect 619

620 In this final section of GCM results we present how  $\lambda_{hist}$  and the pattern effect varies on decadal  
621 timescales in the *amip-piForcing* and *hadSST-piForcing* simulations.

622 Following Gregory and Andrews (2016) we calculate  $\lambda_{hist} = dN/dT$  over a moving 30 year window in  
623 the *amip-piForcing* and *hadSST-piForcing* simulations (Figure 6a and b). For example  $\lambda_{hist}$  calculated  
624 over the 30 year period 1925 to 1954 is presented at year 1939.5 in Figure 6. In Figures 6c-h the LW  
625 and SW clear-sky and cloud radiative effect of the feedback are also shown. The correlation  
626 coefficient between the *amip-piForcing* and *hadSST-piForcing* multi-model-mean  $\lambda_{hist}$  timeseries is  
627 0.84, suggesting the broad features of the decadal  $\lambda_{hist}$  variations are robust to the SST datasets. In  
628 particular  $\lambda_{hist}$  peaks (least negative, smallest pattern effect) around 1940 while generally being large  
629 in magnitude (large pattern effect) over recent decades (see also Gregory and Andrews, 2016; Zhou  
630 et al. 2016; Andrews et al. 2018; Gregory et al. 2020). The clear sky feedbacks (Figures 6c-f) are  
631 largely stable, while the variation in  $\lambda_{hist}$  is almost entirely explained by variation in cloud feedback  
632 (Figures 6g-h), consistent with previous findings (e.g. Zhou et al. 2016; Andrews et al. 2018).

633 In Section 5, we discuss further the reasons for the decadal variations in SST patterns and  $\lambda_{hist}$ , i.e.  
634 whether they are the result of spatiotemporal changes in forcings such as aerosols or volcanic  
635 forcing or due to unforced variability.

636

637

#### 638 4. Observed climate change

639 We next consider whether the radiative feedback and pattern effects simulated by the GCMs are  
640 consistent with observed variations in the Earth’s energy budget. Gregory et al. (2020) asked a  
641 similar question for the post 1980 period and suggested they are (see their Figure 5c), but here we  
642 go a few steps further. Specifically, not only do we consider the post 1980 period, but also assess  
643 changes in the Earth’s energy budget back to the 1800s. Furthermore we investigate the implications  
644 of a strongly negatively feedback parameter (large pattern effect) since 1985 on the observed rate of  
645 global warming.

646 The observations also provide an opportunity to bring our  $\lambda_{\text{hist}}$  and pattern effect estimate up to date  
647 with the most recently observed data (up to and including 2019), whereas our GCM analysis  
648 generally finished in 2014. The observations post 2014 period are of particular interest given they  
649 include the major El-Nino event of 2015/2016 that was associated with eastern-pacific warming and  
650 marked changes in the observed radiation budget (Loeb et al. 2020; 2021). We expect these post  
651 2014 years to have an impact  $\lambda_{\text{hist}}$  and the pattern effect, given the process understanding discussed  
652 previously (e.g. Zhou et al., 2016, Andrews and Webb, 2018, Ceppi and Gregory, 2017; Dong et al.  
653 2019).

##### 654 4.1 Comparison of AGCM results to observed estimates

655 We first validate the AGCM  $\lambda_{\text{hist}}$  estimates over recent decades. To do this we use a merged satellite  
656 dataset (ERBE WFOV + CERES) (Allan et al. 2014) that provides an observational estimate of  $dN$   
657 variations from 1985 to 2019. For  $dT$  we use the HadCRUT5 analysis dataset (Morice et al. 2021). For  
658  $dF$  we use the IPCC AR6 (Forster et al. 2021) best estimate historical ERF changes. These datasets are  
659 described in further detail in Section 2.4. We first consider the 30-year period 1985 to 2014,  
660 consistent with many of the AGCMs.

661 Figure 7a and 7b show the  $dT$ ,  $dN$  and  $dF$  timeseries over this period. The 1985-2014 ‘observed’  $-\lambda_{\text{hist}}$   
662  $= d(F - N)/dT \sim 2.0 \pm 0.7 \text{ W m}^{-2} \text{ K}^{-1}$  relationship is shown in Figure 7d. Note the stated 5-95%  
663 uncertainty is  $\pm 1.645\sigma$  from the standard error of the linear fit, with no allowance for systematic  
664 uncertainties. As discussed in Section 2.4, observed multi-decadal changes in  $dN$  are subject to a  
665 substantial uncertainty (up to  $0.5 \text{ W m}^{-2}$ ) primarily related to the breaks in the record prior to 2000,  
666 though are considerably smaller afterwards (Liu et al. 2020). Note also that years 1991-2 are  
667 excluded from the calculation as these years are identified as being strongly impacted by the  
668 volcanic forcing from the Pinatubo eruption (Figure 7b). Whilst  $\lambda_{\text{hist}}$  is robust to this (we get just the  
669 same  $\lambda_{\text{hist}} \sim -2.0 \pm 0.7 \text{ W m}^{-2} \text{ K}^{-1}$  if we include these years), including these years has an impact on the  
670 ocean heat uptake efficiency estimate (see Section 4.3). The observed 1985-2014  $\lambda_{\text{hist}}$  estimate is  
671 shown on Figure 6a and 6b (red line) as an illustration in comparison to the AGCM decadal variations  
672 in  $\lambda_{\text{hist}}$ . The observed  $\lambda_{\text{hist}}$  best estimate agrees exceptionally well with the AGCM multi-model mean,  
673 and nearly all models are within the 5-95% uncertainty estimate as they approach the 1985-2014  
674 value (Figure 6a and 6b).

675 A more rigorous comparison of individual AGCM results to the observed estimate is shown in Figure  
676 8. Here the AGCM  $\lambda_{\text{hist}}$  estimates from *amip-piForcing* and *hadSST-piForcing* have been calculated in  
677 the same way as the observations, i.e. over 1985-2014 excluding 1991-2. The overlap between the  
678 model and observed estimates points to broad consistency between the models and observations in  
679 the recent decadal value of  $\lambda_{\text{hist}}$  (Figure 8). The large uncertainties (which are likely underestimated  
680 since we have not accounted for structural errors) inhibit a more precise validation of individual  
681 models against the observed estimate.

682 For the full the historical record we estimate  $\lambda_{\text{hist}}$  from IPCC AR6 assessed changes in  $T$ ,  $N$  and  $F$ .  
683 Forster et al. (2021) give these as  $\Delta T = 1.03 \pm 0.20$  K,  $\Delta N = 0.59 \pm 0.35$  W m<sup>-2</sup> and  $\Delta F = 2.20$  [1.53 to  
684 2.91] W m<sup>-2</sup> for the time-period 1850-1900 to 2006-2019. For simplicity we assume  $\Delta F = 2.20 \pm 0.7$  W  
685 m<sup>-2</sup>, where we have approximated the uncertainty in  $\Delta F$  as a Gaussian. Randomly sampling (with  
686 replacement) from the Gaussian distributions in  $\Delta N$ ,  $\Delta F$  and  $\Delta T$  gives  $\lambda_{\text{hist}} = (\Delta N - \Delta F)/\Delta T = -1.6 \pm 0.8$   
687 W m<sup>-2</sup> K<sup>-1</sup>. This is again in agreement with the *amip-piForcing* ( $\lambda_{\text{hist}} = -1.65 \pm 0.46$  W m<sup>-2</sup> K<sup>-1</sup>, Table 2)  
688 and *hadSST-piForcing* ( $\lambda_{\text{hist}} = -1.43 \pm 0.43$  W m<sup>-2</sup> K<sup>-1</sup>, Table 2) 1871-2010 ensembles, though an exact  
689 match is not expected given the slightly different time-periods and methods (e.g. finite differences  
690 versus regression) used. Still, the agreement provides further confidence in the GCM's simulated  
691 radiative response to observed SST and sea-ice variations over the historical record, and strengthens  
692 the conclusion that  $\lambda_{\text{hist}}$  has become more negative over recent decades compared to the longer  
693 1871-2010 time-period.

694 Finally, IPCC AR6 assessed the long-term ECS relevant feedback parameter (analogous to our  $\lambda_{4\times\text{CO}_2}$ )  
695 to be  $-1.16 \pm 0.65$  W m<sup>-2</sup> K<sup>-1</sup> (Forster et al., 2021) by combining lines of evidence from observations,  
696 theory, process models and GCMs on individual climate feedback processes. Combining this with our  
697 observed  $\lambda_{\text{hist}}$  estimates above gives an estimate of the pattern effect independently of our GCM  
698 ensemble. This gives an estimated pattern effect of  $\sim 0.8 \pm 1.0$  W m<sup>-2</sup> K<sup>-1</sup> for 1985-2015 and  $\sim 0.4 \pm 1.1$   
699 W m<sup>-2</sup> K<sup>-1</sup> for the full historical record (the 1850-1900 to 2006-2019 changes). While the uncertainties  
700 are substantial, there is again agreement with our GCM results.

#### 701 4.2 Recent observed trends and the efficiency of ocean heat uptake

702 We have seen that both models and observed variations in the Earth's energy budget agree on the  
703 Earth having had strongly stabilizing feedbacks over recent decades relative to AOGCM feedbacks  
704 under long-term CO<sub>2</sub> forced climate change. Quantifying this in a different way, a feedback  
705 parameter of  $\sim -2.0$  W m<sup>-2</sup> K<sup>-1</sup> suggests an EffCS =  $-F_{2\times}/\lambda_{\text{hist}}$  as low as  $\sim 4.0/2.0 \sim 2.0$  K operating over  
706 1985-2014, assuming  $F_{2\times} = 4.0$  W m<sup>-2</sup> (Sherwood et al. 2020). From this it seems possible that the  
707 rate of global warming over this period ( $\sim 0.19$  K dec<sup>-1</sup>, Tokarska et al., 2020) might have been larger  
708 had the Earth warmed over this period with a pattern of SST associated with more positive  
709 feedbacks, as found in earlier parts of the historical record (Section 3). However, we also investigate  
710 the possibility that changes in ocean heat uptake efficiency may have compensated the changes in  
711 feedbacks and low EffCS to maintain the higher warming rate over this period.

712 To do this we turn to the 'climate resistance' ( $\rho$ , units W m<sup>-2</sup> K<sup>-1</sup>) "zero-layer" model of Gregory and  
713 Forster (2008) to analyse the ocean heat uptake efficiency ( $\kappa$ , units W m<sup>-2</sup> K<sup>-1</sup>). This is expressed as  
714  $dF = \rho dT$ , where  $\rho = \kappa - \lambda$ , and  $\kappa$  is defined as  $\kappa = dN/dT$  and is found to be strongly related to the  
715 thermal coupling constant ( $\gamma$ , units W m<sup>-2</sup> K<sup>-1</sup>) between the upper and lower ocean in the two-layer  
716 model (Gregory et al. 2015; see their Figure 8). While the zero-layer model is a gross simplification of  
717 the climate system (we discuss potential limitations below),  $dF = \rho dT$  is found to be an excellent  
718 approximation ( $r=0.86$ ) over 1985 – 2014 (excluding the 1991-2 Pinatubo years, see below) in our  
719 data (Figure 7c). From this relationship we deduce  $\rho = dF/dT \sim 2.4 \pm 0.5$  W m<sup>-2</sup> K<sup>-1</sup> over 1985-2014  
720 (Figure 7c) and similarly  $\kappa = dN/dT \sim 0.4 \pm 0.8$  W m<sup>-2</sup> K<sup>-1</sup>. In contrast, AOGCM simulations of steady  
721 increasing CO<sub>2</sub> generally have a larger ocean heat uptake efficiency ( $\kappa = 0.73 \pm 0.18$  W m<sup>-2</sup> K<sup>-1</sup> for  
722 years 61-80 of CMIP5 1%CO<sub>2</sub> AOGCM simulations, Gregory et al., 2015).

723 Another effect on surface temperature to consider is the possibility that the pattern of surface  
724 warming and/or atmospheric circulation may change the efficiency of global heat uptake, thus not  
725 only is  $\lambda$  inconstant, but  $\kappa$  may also vary too. Using passive ocean uptake experiments wherein  
726 ocean circulation cannot change, Newsom et al. (2020) find that ocean heat uptake efficiency can be

727 expected to be smaller when warming is enhanced in the tropics (where deep ocean ventilation is  
728 small) and larger when warming is enhanced in the high latitudes (where deep ocean ventilation is  
729 large). With relatively small warming in the southern high latitudes, this suggests that the  
730 surface/ocean-mixed layer might have been less efficient at fluxing heat into the deep ocean over  
731 the same period as the large pattern effect, potentially enhancing global surface warming and  
732 muting some of the impact of feedback changes. However, stronger trade winds, as have been  
733 observed over 1981-2010, can also be expected to accelerate subtropical cells, enhancing ocean  
734 heat uptake efficiency and slowing global surface warming (England et al. 2014), an effect not  
735 accounted for in the passive ocean heat uptake experiments of Newsom et al. (2020). Thus,  
736 variations in both radiative feedbacks and ocean heat uptake appear to be physically linked through  
737 SST patterns and may even to some extent co-vary (Newsom et al. 2020).

738 As our  $dN$  timeseries does not predate 1985 we cannot investigate whether  $\kappa$  has varied in a way  
739 that would counter changes in  $\lambda_{\text{hist}}$  prior to 1985. Instead, we go forward in time exploiting the  
740 datasets up to and including 2019. This includes the major El-Nino event of 2015/2016 and marked  
741 changes in the observed radiation budget (Loeb et al. 2020; 2021). Figure 9 illustrates the impact of  
742 this event on the pattern of decadal surface warming trends. Over 1985-2014 there is marked  
743 cooling over the eastern Pacific (Figure 9a) which is much reduced when the pattern is calculated  
744 over 1987-2016 (Figure 9b) to include the peak 2015-16 El-Nino years. The difference (Figure 9c)  
745 shows the warming event of the 2015-16 El-Nino on the eastern Pacific, while cooling in the western  
746 Pacific, as well as a slight reduction in Southern Ocean cooling. This is precisely the pattern of SST  
747 change we'd expect to have an impact on  $\lambda$ .

748 Table 4 shows the impact on 30-year derived  $\rho$ ,  $\lambda$  and  $\kappa$  values moving forward in time from 2014, up  
749 to and including 1990-2019. Figure 7 (red crosses) shows these additional 5 years in comparison to  
750 the 1985-2014  $\rho$  and  $\lambda$  relationships. Post 2014,  $\lambda$  reduces in magnitude (Table 4) and all the red  
751 crosses fall below the 1985-2014  $\lambda$  relationship in Figure 7d. This is consistent with process based  
752 arguments that the shift to eastern Pacific warming post 2014 ought to drive more positive  
753 feedbacks and consequently a reduction of the pattern effect over these years. If the AGCM  
754 simulations were extended to cover this time-period we ought to expect them to simulate a similar  
755 response. This would be worthwhile future work complementary to Loeb et al. (2020).

756 In contrast to  $\lambda$ ,  $\rho$  is relatively stable to these additional years (Table 4) and the 1985-2014  $\rho$   
757 relationship is found to be an excellent predictor for 2015-2019 (red crosses fall on or close to the  
758 line, Figure 7c). A consequence of  $\rho$  being well approximated as constant but  $\lambda$  not, is that  $\kappa$  (equal to  
759  $\rho + \lambda$ ) must compensate for the change in  $\lambda$ . Thus beyond 2014, the pattern effect declines but its  
760 impact on surface temperature is buffered by a change in ocean heat uptake efficiency. This is  
761 consistent with the original hypothesis that variations in SST patterns affect both heat loss to space  
762 (radiative feedbacks) and the efficiency of heat uptake into the deep-ocean in a way that might co-  
763 vary (Newsom et al., 2020). However, the extent of any anti-correlation is unclear, it may simply  
764 apply to short term variability. It clearly does not apply to longer-term forced changes, given that  
765 Gregory et al. (2015) found substantial variations in  $\rho$ , which would not occur if  $\kappa$  and  $\lambda$  were  
766 strongly anti-correlated.

767 While the zero-layer model appears to work well on this short timescale (Figure 7c) we caution  
768 against assuming all changes in ocean heat content are driven by global  $T$ , as assumed by the  $dN =$   
769  $\kappa dT$  relationship. This is because, especially on short timescales, other influences that do not  
770 correlate with global  $T$ , such as wind-driven ocean circulation changes perhaps, will also alter ocean  
771 heat content (England et al., 2014). In such a situation, it would be reasonable to write  $N = \kappa T + U$   
772 where  $U$  is an additional term to the heat balance, not related to global  $T$ . This implies  $\kappa = N/T - U/T$ ,

773 and including this term in the forced heat balance,  $N = F + \lambda T + U$ , gives  $\lambda = (N-F)/T - U/T$ . Thus  $U/T$   
774 would perturb the estimate of  $\kappa$  (a positive number) and  $\lambda$  (a negative number) in opposite  
775 directions, as we see in our data. Hence our results are potentially evidence for variation in ocean  
776 heat content not driven by global  $T$ , but we cannot say exactly what it is – other than it does not  
777 scale with global  $T$ .

778 We caution that structural errors could impact on our diagnosis. Specifically, both  $\kappa$  and  $\lambda$  are related  
779 to  $dN$  and so any bias or error in the observed  $dN$  trend would bias  $\kappa$  and  $\lambda$  in opposite directions.  
780 Moreover  $\rho = dF/dT$  would be unaffected by any bias or error in  $dN$ , and so the anti-correlation would  
781 compensate to leave  $\rho = \kappa - \lambda$  unaffected. We illustrate this in Table 4, which shows these quantities  
782 calculated over 1985-2014 using 5 available different versions of the DEEP-C  $dN$  datasets (see  
783 Section 2.4). Differences in the results emerge ( $\lambda$  reduces in magnitude from  $\sim -2.2 \text{ Wm}^{-2} \text{ K}^{-1}$  to  $\sim -2.0$   
784  $\text{Wm}^{-2} \text{ K}^{-1}$ , with a compensating increase in  $\kappa$ ) as the DEEP-C datasets transition from v3 to v4 (i.e. v2  
785 and v3 give the same results, as do v4 and v5), highlighting the impact of potential structural errors  
786 in these results. We do not pursue the cause of the difference in the results, but it is likely due to  
787 changes between v3 and v4 in how the DEEP-C method bridges the gap between satellite products in  
788 the 1990s (a longer adjustment period and a different modelling ensemble is used) (Liu et al., 2020).  
789 However it is also important to note that the observational record since 2000, applying the CERES  
790 dataset, is subject to much smaller structural uncertainty than the earlier record implying a greater  
791 confidence in our analysis of the anomalous  $N$  variations post 2014.

#### 792 *4.3 Effect of the Pinatubo volcanic eruption*

793 Finally, we comment on the effect of the Pinatubo volcanic eruption on these results. There is a large  
794 negative spike in  $dF$  and  $dN$  around 1991 and 1992 (Figure 7b). While we found no impact of these  
795 years on our estimate of 1985 – 2014  $\lambda_{\text{hist}}$ , they have a strong impact on  $\rho$  and  $\kappa$ . Including these  
796 years in the regression analysis, we find  $\rho = dF/dT \sim 2.9 \pm 0.7 \text{ W m}^{-2} \text{ K}^{-1}$  and  $\kappa = dN/dT \sim 0.8 \pm 0.9 \text{ W}$   
797  $\text{m}^{-2} \text{ K}^{-1}$ , much larger than when these years are excluded from the analysis as above. This is  
798 consistent with Gregory et al. (2015) who found the ‘transient climate response parameter’ (equal to  
799  $1/\rho$ , units  $\text{K W}^{-1} \text{ m}^2$ ) to explosive eruptions to be smaller ( $\rho$  larger) than that evaluated in AOGCMs  
800 under steadily increasing  $\text{CO}_2$ , principally because the surface/mixed-layer readily gives up heat ( $\kappa$   
801 larger) in response to a short-lived forcing like an explosive volcanic eruption. Hence if the time-  
802 period under consideration contains large volcanic eruptions then the “zero-layer” model ( $dF = \rho dT$ )  
803 is found to be a poor approximation (i.e.  $\rho$  not constant) over the entire time-period because it  
804 neglects the importance of the upper-ocean heat capacity on short timescales (Gregory and Forster,  
805 2008; Held et al. 2010; Gregory et al., 2016). This manifests itself as a sensitivity of  $\rho$  and  $\kappa$  to the  
806 inclusion or exclusion of volcanic years, as we have found here.

807

## 808 **5. Summary, Discussion and Conclusions**

### 809 *5.1 Historical feedbacks and the pattern effect*

810 The dependence of radiative feedback on the pattern of SST change was investigated in fourteen  
811 Atmospheric General Circulation Models (AGCMs) forced with observed variations in sea-surface-  
812 temperature (SST) and sea-ice over the historical record from 1871 to near-present (*amip-piForcing*  
813 experiment). We found that the pattern effect identified in a previous model intercomparison  
814 (Andrews et al, 2018) is largely robust to a wider set of new generation AGCMs with a broader range  
815 of atmospheric physics and climate sensitivities. Our qualitative conclusions were not strongly  
816 dependent on the AMIP II SST dataset used to force the AGCMs; indeed, the feedbacks in eight

817 AGCMs using SSTs from HadISST1 (*hadSST-piForcing*) were found to be strongly correlated with  
818 feedbacks in *amip-piForcing*, though the magnitude of the pattern effect post 1980 was found to be  
819 smaller under HadISST1 SSTs (see also Andrews et al., 2018; Lewis and Mauritsen, 2021; Zhou et al.,  
820 2021; Fueglistaler and Silvers, 2021).

821 Separating the historical record at 1980, we found that over 1871-1980 the Earth warmed with a  
822 relatively uniform warming pattern and feedbacks largely consistent and strongly correlated with  
823 long-term *abrupt-4xCO2* feedbacks (i.e. with relatively small pattern effect - Figures 2 and 5). In  
824 contrast, post 1980 the Earth warmed with a strong tropical Pacific SST gradient (Figure 4) where  
825 regions of deep convection warm substantially more than the tropical mean (Fueglistaler and Silvers,  
826 2021). This drove large negative feedbacks and pattern effects in both our *amip-piForcing* and  
827 *hadSST-piForcing* simulations, consistent with the physical understanding of how lapse-rate and  
828 cloud feedbacks depend on tropical Pacific SST patterns (Zhou et al., 2016; Andrews and Webb,  
829 2018; Ceppi and Gregory, 2017; Dong et al., 2019).

830 As well as a large pattern effect, feedbacks post 1980 were found to be uncorrelated with long term  
831 CO<sub>2</sub> driven feedbacks (Figure 5). This is unfortunate, because the feedback inferred from this period  
832 therefore does not constrain the CO<sub>2</sub> feedback or ECS. It is also surprising, because the period since  
833 ~1980 contains a well observed large global temperature response, which AOGCMs attribute to  
834 increasing greenhouse gases, and it avoids the aerosol forcing uncertainty issue (Jiménez-de-la-  
835 Cuesta and Mauritsen, 2019). Despite this, it turns out to be the worst period for inferring the  
836 Earth's long-term CO<sub>2</sub> climate sensitivity from the observed global energy balance. Conversely,  
837 feedbacks acting earlier in the record (1871-1980) are representative of the long-term response (i.e.  
838 smaller pattern effect) and do correlate with  $\lambda_{4xCO_2}$  across models, yet this period has a smaller  
839 climate change signal and is not as well observed, containing much larger uncertainties relative to  
840 the climate change signal (e.g. Otto et al., 2013), as well as a large forcing uncertainty. Hence the  
841 usefulness of this time-period is limited for setting a constraint on  $\lambda_{hist}$ .

842 Considering the historical record as a whole is useful for informing studies that use the entire  
843 observed record to estimate ECS via energy budget constraints (e.g. Sherwood et al. 2020). We  
844 found that the pattern effect over 1871-2010 to be  $\Delta\lambda = 0.70 \pm 0.47 \text{ W m}^{-2} \text{ K}^{-1}$  in our *amip-piForcing*  
845 ensemble and  $\Delta\lambda = 0.44 \pm 0.31 \text{ W m}^{-2} \text{ K}^{-1}$  in *hadSST-piForcing*, where the smaller uncertainty in  
846 *hadSST-piForcing* likely reflects the narrower set of model physics in this smaller ensemble (we do  
847 not have *hadSST-piForcing* experiments for the models with either the largest (CESM2) or smallest  
848 (MIROC6) pattern effects in *amip-piForcing*). The question therefore arises as to which of these  
849 estimates ought to be used for adjusting historical energy budget constraints on ECS for pattern  
850 effects.

851 Both Lewis and Mauritsen (2021) and Fueglistaler and Silvers (2021) showed that the AMIP II dataset  
852 had the largest warm pool trends relative to the tropical-mean of all SST reconstructions they  
853 considered. Hence one interpretation of our results is that the pattern effect in *amip-piForcing* might  
854 usefully be regarded as an upper bound on the structural uncertainty of the experimental design to  
855 observational uncertainty in SST reconstructions. A best estimate might place more weight on the  
856 *hadSST-piForcing* pattern effects, which have warm pool trends (relative to the tropical-mean) closer  
857 to the middle of the range of SST reconstructions (Fueglistaler and Silvers, 2021; Lewis and  
858 Mauritsen, 2021). In that case, we recommend a best estimate of the historical pattern effect of  
859  $0.44 \pm 0.47 \text{ W m}^{-2} \text{ K}^{-1}$  for the time-period 1871-2010, which represents the pattern effect from  
860 *hadSST-piForcing* but retaining the larger uncertainty from the (larger ensemble) *amip-piForcing*  
861 results. If calculated over 1871-2014 the pattern effect increases by  $0.05 \pm 0.04 \text{ W m}^{-2} \text{ K}^{-1}$  according  
862 to the *hadSST-piForcing* ensemble. This best estimate of the historical pattern effect is close to that

863 used in Sherwood et al. (2020), who assumed a value of  $0.5 \pm 0.5 \text{ W m}^{-2} \text{ K}^{-1}$  (they were informed by  
864 Andrews et al. (2018) but allowed for a potentially smaller pattern effect than that study based on  
865 expert judgement). In the future, a model intercomparison of the pattern effect to a broader range  
866 of SST datasets would be useful to address any outstanding structural uncertainty to SST  
867 reconstructions.

868 To provide independent evidence for the historical pattern effect, we used IPCC AR6 assessed  
869 changes in  $T$ ,  $N$  and  $F$  between 1850-1900 to 2006-2019 (Forster et al. 2021) to estimate a historical  
870 feedback parameter of  $\lambda_{\text{hist}} = (\Delta N - \Delta F)/\Delta T = -1.6 \pm 0.8 \text{ W m}^{-2} \text{ K}^{-1}$ . This was found to be in agreement  
871 with the *amip-piForcing* and *hadSST-piForcing* ensembles. IPCC AR6 also assessed the long-term ECS  
872 relevant feedback parameter ( $-1.16 \pm 0.65 \text{ W m}^{-2} \text{ K}^{-1}$ , Forster et al., 2021) from combining lines of  
873 evidence from observations, theory, process models and GCMs on individual climate feedback  
874 processes. Contrasting this with the  $\lambda_{\text{hist}}$  estimate above gives an estimate of the pattern effect of  $0.4$   
875  $\pm 1.1 \text{ W m}^{-2} \text{ K}^{-1}$  for historical changes between 1850-1900 to 2006-2019. While the uncertainties are  
876 substantial, this is in agreement with our GCM based estimate of the historical pattern effect.

### 877 5.2 Observed climate change since 1985 and ocean heat uptake efficiency

878 Satellite based reconstructions of the Earth's energy balance over 1985 to 2014 suggest a feedback  
879 parameter of  $\sim -2.0 \pm 0.7 \text{ W m}^{-2} \text{ K}^{-1}$ , in agreement with our *amip-piForcing* and *hadSST-piForcing*  
880 ensembles. Evidence is also emerging from satellite records in support of the physical processes and  
881 mechanisms of the pattern effect between surface temperature, atmospheric stability, cloudiness  
882 and radiative fluxes over recent decades (e.g. Zhou et al., 2016; Ceppi and Gregory, 2017; Loeb et al.,  
883 2020; Fueglistaler and Silvers, 2021; Ceppi and Fueglistaler, 2021).

884 Extending our analysis post 2014 included the major El-Nino event of 2015/2016 that was associated  
885 with eastern-pacific warming and marked changes in the observed radiation budget (Loeb et al.  
886 2020; 2021). Including these post 2014 years (up to and including 2019) reduced the magnitude of  
887 the observed  $\lambda$  estimate, consistent with eastern Pacific warming driving more positive feedbacks (as  
888 also suggested in Loeb et al., 2020). This suggests the pattern effect that has existed over recent  
889 decades may be waning if a shift from western to eastern Pacific warming is maintained in the  
890 longer term, as might be expected from a change in the PDO index identified by Loeb et al. (2020).

891 Given the substantial rate of global warming since 1985, what does the presence of a large pattern  
892 effect imply for ocean heat uptake efficiency ( $\kappa$ )? We estimated  $\kappa = dN/dT \sim 0.4 \pm 0.8 \text{ W m}^{-2} \text{ K}^{-1}$  over  
893 1985-2014, which is smaller (but not necessarily inconsistent) with AOGCM simulations of steady  
894 increasing  $\text{CO}_2$  ( $\kappa = 0.73 \pm 0.18 \text{ W m}^{-2} \text{ K}^{-1}$  for years 61-80 of CMIP5 1% $\text{CO}_2$  AOGCM simulations,  
895 Gregory et al. 2015). It raises the possibility that the pattern of surface warming and/or atmospheric  
896 circulation may also change the efficiency of global heat uptake, thus both  $\lambda$  and  $\kappa$  might vary and to  
897 some extent be related (Newsom et al., 2020). If an anti-correlation existed, it could buffer the  
898 impact of a large pattern-effect on transient climate change.

899 We found that despite the change in radiative feedback post 2014 when the eastern Pacific warmed,  
900 the climate resistance  $\rho = dF/dT = \kappa - \lambda$  remained approximately constant, suggesting that  $\kappa$  and  $\lambda$   
901 co-varied. We showed that this result is potential evidence for a change in ocean heat content not  
902 driven by global  $T$ . While this result is suggestive, the extent of this compensation and timescales it  
903 applies to remains unclear. It may simply apply to short term variability and clearly does not apply to  
904 longer-term forced changes (e.g. Gregory et al., 2015). Future research investigating how ocean  
905 uptake efficiency and atmospheric radiative feedbacks are linked through patterns of SST change  
906 would be useful.

907 5.4 Outlook and Implications for AOGCMs

908 Our results raise important questions for studies that have used emergent relationships from  
909 AOGCMs to constrain ECS from recently observed decadal warming since ~1980 (e.g. Jiménez-de-la-  
910 Cuesta and Mauritsen, 2019; Tokarska et al., 2020; Nijse et al., 2020).

911 Firstly, how is it possible that AOGCMs produce an emergent relationship between their recent  
912 decadal warming trends and their ECS, while our results suggest that recent decadal feedbacks  
913 ought to be unrelated to ECS? One solution to this conundrum is provided by Fueglistaler and Silvers  
914 (2021), who showed that AOGCMs typically do not simulate the recent configuration of tropical  
915 Pacific SST patterns that gave rise to the recent pattern effect (though some models do have broad  
916 agreements, e.g. Olonscheck et al. 2021, Watanabe et al. 2021). Instead, the pattern of warming in  
917 AOGCMs (and thus feedbacks) over recent decades is more similar to that seen in their *abrupt-*  
918 *4xCO2* simulations (Gregory et al., 2020; Dong et al. 2021). Hence AOGCMs are generally biased in  
919 their simulation of the recent decadal feedbacks and the pattern effect, compared to their  
920 equivalent AGCMs forced with observed SST variations, as shown in Gregory et al. (2020) and Dong  
921 et al. (2021).

922 If AOGCMs are biased in their simulation of recent decadal feedbacks and the pattern effect, it  
923 suggests they may be biased toward simulating recent decadal temperature trends that are too high;  
924 in turn, this would bias emergent constraints that use them toward values of ECS that are too low.  
925 Alternatively, those models that do match the observed warming trend may do so via a  
926 compensation of processes: too small a pattern effect balanced against too large a heat uptake into  
927 the deep-ocean. Some evidence for the potential of this compensating behaviour is provided by  
928 Hedemenn et al. (2017). Analysing the origins of decadal temperature variability in models, they  
929 demonstrated an anti-correlation between the TOA radiative flux and deep-ocean (defined as below  
930 100m) flux contributions to the model's surface layer and decadal temperature trends (see their  
931 Figure 3). In other words, when the TOA radiative flux is in such a configuration to reduce its  
932 contribution to the surface layer, then the surface/mixed-layer taps into the deep-ocean to  
933 compensate for this loss, and vice versa. We speculate that such a configuration of TOA radiative flux  
934 is potentially consistent with a large negative feedback, since in this configuration of atmospheric  
935 feedbacks the surface efficiently radiates heat back to space. This again suggests a potential anti-  
936 correlation between the ocean heat uptake efficiency and  $\lambda$  during unforced decadal variability  
937 timescales as discussed previously.

938 Going forward, a critical question for future research is to understand what caused the particular  
939 configuration of SST patterns over recent decades (e.g. strong warming in the western Pacific while  
940 cooling in the eastern Pacific and Southern Ocean, despite temperature increasing in the global-  
941 mean; Figure 4 and 9), and how might this pattern evolve in the future. For example, various  
942 hypotheses have been put forward:

- 943 1. It could represent a mode of unforced coupled atmosphere-ocean variability (e.g.  
944 Xie et al., 2016; Watanabe et al. 2021), albeit an unusual one is that is rarely  
945 simulated by AOGCMs (Fueglistaler and Silvers, 2021). In this scenario, we might  
946 expect the pattern effect to reduce in the near-future as the configuration of  
947 tropical SST patterns shift to more warming in the east than the west. There is some  
948 evidence (Loeb et al. 2020; 2021) this has already begun to happen in the most  
949 recent years, as we have also shown. We might therefore, expect an acceleration of  
950 warming trends, unless the additional heat at the surface from the reduced pattern



951 effect is tempered by compensating heat exchanges with the deep-ocean  
952 (Hedemann et al. 2017).

- 953 2. Spatiotemporal variations in anthropogenic forcings such as aerosols (e.g., Smith et  
954 al., 2015; Takahashi & Watanabe, 2016; Moseid et al., 2020; Heede and Fedorov,  
955 2021) or explosive volcanic eruptions (Smith et al. 2015; Gregory et al. 2020) have  
956 been implicated in driving tropical Pacific SST patterns. In these scenarios, the  
957 pattern effect may decline with the reduction in aerosol emissions in the future, or  
958 continue to have decadal variations associated with future volcanism. Whether  
959 changes in deep-ocean fluxes will be accompanied with such forced changes in the  
960 pattern effect is unclear.
- 961 3. While not explaining the eastern Pacific cooling per se, a delayed warming in the  
962 eastern Pacific relative to the west is an expected transient response to forcing due  
963 to the upwelling of (as yet) unperturbed waters from below (Clement et al., 1993;  
964 Held et al. 2010; Heede and Fedorov, 2021). The implication of this is that  
965 eventually the eastern Pacific will warm, and hence we might expect the pattern  
966 effect to reduce and the Earth to warm with stronger (positive) cloud feedbacks.
- 967 4. In contrast, AOGCMs may overstate the expected warming in the eastern Pacific  
968 (e.g. Seager et al., 2020). Under this scenario, we might expect the pattern effect to  
969 reduce after the eastern Pacific stops cooling, but the full pattern effect according  
970 to AOGCMs may never materialise if they incorrectly simulate a strong 'ENSO-like'  
971 pattern in their long-term response to CO<sub>2</sub>. However, a lack of eastern Pacific  
972 warming in the long-term seems unlikely according to paleoclimate records (Tierney  
973 et al. 2019; 2020).
- 974 5. Teleconnections from either the Atlantic Ocean (McGregor et al. 2018) or Southern  
975 Ocean (Hwang et al. 2017) have potentially driven the tropical Pacific SST patterns.  
976 Under the scenario of an Atlantic influence, we might expect the pattern effect to  
977 reduce as Atlantic SST trends evolve over the next few decades. Under the scenario  
978 of a Southern Ocean influence, we might expect the pattern effect to reduce as the  
979 Southern Ocean surface warms; this could take years to decades if the Southern  
980 Ocean temperature trends have been largely mediated by internal variability (e.g.,  
981 Zhang et al. 2019) but could take centuries or longer if Southern Ocean cooling  
982 continues due, for instance, to freshwater input from ongoing Antarctic ice shelf  
983 melt (e.g., Sadai et al. 2020).

984 These are merely some of the proposed hypotheses, and not meant to be an exhaustive list. But  
985 whatever the reason, the fact that AOGCMs rarely simulate this pattern (e.g. Watanbe et al., 2021;  
986 Fueglistaler and Silvers, 2021; Dong et al., 2021) is a concern, suggesting either that their unforced  
987 decadal variability is deficient, or that their forced response is biased, and in either case there is a  
988 serious systematic error which affects all AOGCMs. Moreover, each of the above interpretations  
989 imply different futures, and therefore untangling them is critical for informing both near-term and  
990 long-term climate projections. This is time critical because satellite evidence suggests the Pacific SST  
991 pattern that has dominated recent decades is currently shifting (Loeb et al., 2020) and indeed the  
992 Earth's energy balance is rapidly changing with it (Loeb et al. 2021; Raghuraman et al., 2021).  
993 Predicting the near future therefore depends on maintaining the continuity of the satellite record  
994 and untangling the above mechanisms.

995

996 **Acknowledgements**

997 TA and JMG thank Richard Wood and Mark Ringer for useful discussions. We thank Bosong Zhang,  
998 Zhihong Tan and Knut von Salzen for useful comments on an early draft version of the manuscript.  
999 TA, JMG and ABS were supported by the Met Office Hadley Centre Climate Programme funded by  
1000 BEIS. TA, TM, AM and RR have received funding from the European Union’s Horizon 2020 research  
1001 and innovation programme under grant agreement 820829. JMG’s work is also supported by the  
1002 European Research Council (ERC, grant agreement No 786427, project “Couplet”). TM and AM  
1003 received funding from the European Research Council grant 770765. The contribution of JB to this  
1004 work was funded by the U. S. Department of Energy’s Regional and Global Modeling Analysis  
1005 program area. TO was supported by the Integrated Research Program for Advancing Climate Models  
1006 (TOUGOU) Grant Number JPMXD0717935457 from the Ministry of Education, Culture, Sports,  
1007 Science and Technology (MEXT), Japan. CL was supported by the National Natural Science  
1008 Foundation of China (42075036). KCA and YD acknowledge support from the National Science  
1009 Foundation (Grant AGS-1752796) and from the National Oceanic and Atmospheric Administration  
1010 MAPP Program (Award NA20OAR4310391). BM acknowledges support by the U.S. Department of  
1011 Energy under Award Number DE-SC0022070 and National Science Foundation (NSF) IA 1947282; the  
1012 National Center for Atmospheric Research, which is a major facility sponsored by the NSF under  
1013 Cooperative Agreement No. 1852977; and the National Oceanic and Atmospheric Administration  
1014 under award NA20OAR4310392.

1015

1016 **Data Availability**

1017 Global-annual-ensemble-mean  $dT$  and  $dN$  from all *amip-piForcing*, *hadSST-piForcing* and *abrupt-*  
1018 *4xCO2* simulations are provided here <https://github.com/timothyandrews/amip-hadSST-piForcing>.  
1019 Raw data from CMIP6 *amip-piForcing* simulations (indicated in Table 1) are available at  
1020 <https://pcmdi.llnl.gov/CMIP6/>. *abrupt-4xCO2* raw data for most models is available at CMIP5  
1021 (<https://esgf-node.llnl.gov/projects/cmip5/>) or CMIP6 (<https://pcmdi.llnl.gov/CMIP6/>). The  
1022 HadCRUT5 analysis dataset is available at <https://www.metoffice.gov.uk/hadobs/hadcrut5/>. IPCC  
1023 AR6 ERF timeseries is available at <https://github.com/IPCC-WG1/Chapter-7> (see  
1024 [https://github.com/IPCC-WG1/Chapter-7/blob/main/data\\_output/AR6\\_ERF\\_1750-2019.csv](https://github.com/IPCC-WG1/Chapter-7/blob/main/data_output/AR6_ERF_1750-2019.csv)). DEEP-C  
1025 v5  $dN$  radiative fluxes can be obtained from <https://researchdata.reading.ac.uk/347/> and previous  
1026 versions described at <http://www.met.reading.ac.uk/~sgs02rpa/research/DEEP-C/GRL/>. The  
1027 HadISST1 SSTs used to force the *hadSST-piForcing* simulations are available at  
1028 <https://www.metoffice.gov.uk/hadobs/hadisst/>, see  
1029 [https://www.metoffice.gov.uk/hadobs/hadisst/data/HadISST\\_sst.nc.gz](https://www.metoffice.gov.uk/hadobs/hadisst/data/HadISST_sst.nc.gz).

1030 **References**

- 1031 Allan, R. P., Liu, C., Loeb, N. G., Palmer, M. D., Roberts, M., Smith, D., and Vidale, P.-L. (2014),  
1032 Changes in global net radiative imbalance 1985–2012, *Geophys. Res. Lett.*, 41, 5588– 5597,  
1033 doi:[10.1002/2014GL060962](https://doi.org/10.1002/2014GL060962).
- 1034 Andrews, T., Gregory, J. M., Paynter, D., Silvers, L. G., Zhou, C., Mauritsen, T., Webb, M. J., Armour,  
1035 K. C., Forster, P. M., & Titchner, H. (2018). Accounting for changing temperature patterns increases  
1036 historical estimates of climate sensitivity. *Geophysical Research Letters*, 45, 8490– 8499.  
1037 <https://doi.org/10.1029/2018GL078887>
- 1038 Andrews, T., Gregory, J. M., & Webb, M. J. (2015). The dependence of radiative forcing and feedback  
1039 on evolving patterns of surface temperature change in climate models. *Journal of Climate*, 28, 1630–  
1040 1648.
- 1041 Andrews, T., Gregory, J. M., Webb, M. J., & Taylor, K. E. (2012). Forcing, feedbacks and climate  
1042 sensitivity in CMIP5 coupled atmosphere–ocean climate models. *Geophysical Research Letters*, 39,  
1043 L09712. <https://doi.org/10.1029/2012GL051607>
- 1044 Andrews, T., & Ringer, M. A. (2014). Cloud feedbacks, rapid adjustments, and the forcing–response  
1045 relationship in a transient CO<sub>2</sub> reversibility scenario. *Journal of Climate*, 27(4), 1799– 1818.  
1046 <https://doi.org/10.1175/JCLI-D-13-00421.1>
- 1047 Andrews, T., & Webb, M. J. (2018). The dependence of global cloud and lapse rate feedbacks on the  
1048 spatial structure of tropical Pacific warming. *Journal of Climate*, 31. <https://doi.org/10.1175/JCLI-D-17-0087.1>
- 1050 Annan, J. D., & Hargreaves, J. C. (2017). On the meaning of independence in climate science. *Earth*  
1051 *System Dynamics*, 8, 221– 224.
- 1052 Annan, J. D., & Hargreaves, J. C. (2011). Understanding the CMIP3 Multimodel Ensemble, *Journal of*  
1053 *Climate*, 24(16), 4529-4538. <https://doi.org/10.1175/2011JCLI3873.1>.
- 1054 Armour, K. C. (2017). Energy budget constraints on climate sensitivity in light of inconstant climate  
1055 feedbacks. *Natural Climate Change*, 7, 331– 335. <https://doi.org/10.1038/nclimate3278>
- 1056 Armour, K. C., Bitz, C. M., & Roe, G. H. (2013). Time-varying climate sensitivity from regional  
1057 feedbacks. *Journal of Climate*, 26, 4518– 4534.
- 1058 Boucher, O., Servonnat, J., Albright, A. L., Aumont, O., Balkanski, Y., & Bastrikov, V., et al. (2020).  
1059 Presentation and evaluation of the IPSL-CM6A-LR climate model. *Journal of Advances in Modeling*  
1060 *Earth Systems*, 12, e2019MS002010. <https://doi.org/10.1029/2019MS002010>
- 1061 Bloch-Johnson, J., Rugenstein, M., Stolpe, M. B., Rohrschneider, T., Zheng, Y., & Gregory, J. M.  
1062 (2021). Climate sensitivity increases under higher CO<sub>2</sub> levels due to feedback temperature  
1063 dependence. *Geophysical Research Letters*, 48, e2020GL089074.  
1064 <https://doi.org/10.1029/2020GL089074>
- 1065 Block, K., and Mauritsen, T. (2013), Forcing and feedback in the MPI-ESM-LR coupled model under  
1066 abruptly quadrupled CO<sub>2</sub>, *J. Adv. Model. Earth Syst.*, 5, 676– 691, doi:[10.1002/jame.20041](https://doi.org/10.1002/jame.20041).
- 1067 Bjordal, J., Storelvmo, T., Alterskjær, K. et al., 2022: Equilibrium climate sensitivity above 5 °C  
1068 plausible due to state-dependent cloud feedback. *Nat. Geosci.* **13**, 718–721 (2020).doi,  
1069 10.1038/s41561-020-00649-1.

1070 Caballero, R., & Huber, M. (2013). State-dependent climate sensitivity in past warm climates and its  
1071 implications for future climate projections. *Proceedings of the National Academy of Sciences of the*  
1072 *United States of America*, 110, 14,162– 14,167. <https://doi.org/10.1073/pnas.1303365110>

1073 Ceppi, P., & Gregory, J. M. (2017). Relationship of tropospheric stability to climate sensitivity and  
1074 Earth's observed radiation budget. *Proceedings of the National Academy of Sciences of the United*  
1075 *States of America*, 114, 13,126– 13,131. <https://doi.org/10.1073/pnas.1714308114>

1076 Chalmers, J., Kay, J. E., Middlemas, E. A., Maroon, E. A., & DiNezio, P., 2022: Does disabling cloud  
1077 radiative feedbacks change spatial patterns of surface greenhouse warming and cooling?, *Journal of*  
1078 *Climate* (published online ahead of print 2022;  
1079 <https://journals.ametsoc.org/view/journals/clim/aop/JCLI-D-21-0391.1>)

1080 Collins, M., and Coauthors, 2013: Long-term climate change: Projections, commitments and  
1081 irreversibility. *Climate Change 2013: The Physical Science Basis*, T. F. Stocker et al., Eds., Cambridge  
1082 University Press, 1029–1136.

1083 Clement, A. C., Seager, R., Cane, M. A., & Zebiak, S. E. (1996). An ocean dynamical thermostat.  
1084 *Journal of Climate*, 9, 2190– 2196. [https://doi.org/10.1175/1520-0442\(1996\)009<2,190:AODT>2.0.CO2](https://doi.org/10.1175/1520-0442(1996)009<2,190:AODT>2.0.CO2)

1086 Danabasoglu, G., Lamarque, J.-F., Bacmeister, J., Bailey, D. A., DuVivier, A. K., Edwards, J., et al.  
1087 (2020). The Community Earth System Model Version 2 (CESM2). *Journal of Advances in Modeling*  
1088 *Earth Systems*, 12, e2019MS001916. <https://doi.org/10.1029/2019MS001916>

1089 Dong, Y., Armour, K. C., Proistosescu, C., Andrews, T., Battisti, D. S., Forster, P. M., et al. (2021).  
1090 Biased estimates of equilibrium climate sensitivity and transient climate response derived from  
1091 historical CMIP6 simulations. *Geophysical Research Letters*, 48, e2021GL095778.  
1092 <https://doi.org/10.1029/2021GL095778>

1093 Dong, Y., Armour, K. C., Zelinka, M. D., Proistosescu, C., Battisti, D. S., Zhou, C., & Andrews, T. (2020).  
1094 Inter-model spread in the sea-surface temperature pattern effect and its contribution to climate  
1095 sensitivity in CMIP5 and CMIP6 models. *Journal of Climate*, 33(18), 7755– 7775.  
1096 <https://doi.org/10.1175/JCLI-D-19-1011.1>

1097 Dong, Y., Proistosescu, C., Armour, K. C., & Battisti, D. S. (2019). Attributing historical and future  
1098 evolution of radiative feedbacks to regional warming patterns using a Green's Function approach:  
1099 The preeminence of the western Pacific. *Journal of Climate*, 32(17), 5471– 5491.  
1100 <https://doi.org/10.1175/JCLI-D-18-0843.1>

1101 Donner, L. et al.. (2011). The Dynamical Core, Physical Parameterizations, and Basic Simulation  
1102 Characteristics of the Atmospheric Component AM3 of the GFDL Global Coupled Model CM3,  
1103 *Journal of Climate*, 24(13), 3484-3519.

1104 England, M. H., McGregor, S., Spence, P., Meehl, G. A., Timmermann, A., Cai, W., Gupta, A. S.,  
1105 McPhaden, M. J., Purich, A., & Santoso, A. (2014). Recent intensification of wind-driven circulation in  
1106 the Pacific and the ongoing warming hiatus. *Nature Climate Change*, 4(3), 222– 227.  
1107 <https://doi.org/10.1038/nclimate2106>

1108 Eyring, V., Bony, S., Meehl, G. A., Senior, C. A., Stevens, B., Stouffer, R. J., & Taylor, K. E. (2016).  
1109 Overview of the Coupled Model Intercomparison Project Phase 6 (CMIP6) experimental design and  
1110 organizations. *Geoscientific Model Development*, 9, 1937– 1958. <https://doi.org/10.5194/gmd-9-1937-2016>

- 1112 Fueglistaler, S., & Silvers, L.G. (2021). The peculiar trajectory of global warming. *Journal of*  
 1113 *Geophysical Research: Atmospheres*, 126, e2020JD033629. <https://doi.org/10.1029/2020JD033629>
- 1114 Forster, P., T. Storelvmo, K. Armour, W. Collins, J. L. Dufresne, D. Frame, D. J. Lunt, T. Mauritsen, M.  
 1115 D. Palmer, M. Watanabe, M. Wild, H. Zhang, 2021, The Earth's Energy Budget, Climate Feedbacks,  
 1116 and Climate Sensitivity. In: *Climate Change 2021: The Physical Science Basis. Contribution of Working*  
 1117 *Group to the Sixth Assessment Report of the Intergovernmental Panel on Climate Change* [Masson-  
 1118 Delmotte, V., P. Zhai, A. Pirani, S. L. Connors, C. Péan, S. Berger, N. Caud, Y. Chen, L. Goldfarb, M. I.  
 1119 Gomis, M. Huang, K. Leitzell, E. Lonnoy, J.B.R. Matthews, T. K. Maycock, T. Waterfield, O. Yelekçi, R.  
 1120 Yu and B. Zhou (eds.)]. Cambridge University Press. In Press.
- 1121 Flynn, C. M. and Mauritsen, T.: On the climate sensitivity and historical warming evolution in recent  
 1122 coupled model ensembles, *Atmos. Chem. Phys.*, 20, 7829–7842, [https://doi.org/10.5194/acp-20-](https://doi.org/10.5194/acp-20-7829-2020)  
 1123 [7829-2020](https://doi.org/10.5194/acp-20-7829-2020), 2020.
- 1124 Gates, W. L., Boyle, J. S., Covey, C., Dease, C. G., Doutriaux, C. M., Drach, R. S., et al. (1999). An  
 1125 overview of the results of the Atmospheric Model Intercomparison Project (AMIP I). *Bulletin of the*  
 1126 *American Meteorological Society*, 80(1), 29– 55. [https://doi.org/10.1175/1520-](https://doi.org/10.1175/1520-0477(1999)080<0029:AOTRO>2.0.CO;2)  
 1127 [0477\(1999\)080<0029:AOTRO>2.0.CO;2](https://doi.org/10.1175/1520-0477(1999)080<0029:AOTRO>2.0.CO;2)
- 1128 Geoffroy, O., et al. (2013). Transient climate response in a two-layer energy-balance model. Part II:  
 1129 Representation of the efficacy of deep-ocean heat uptake and validation for CMIP5 AOGCMs.  
 1130 *Journal of Climate*, 26, 1859– 1876.
- 1131 Gregory, J. M., & Andrews, T. (2016). Variation in climate sensitivity and feedback parameters during  
 1132 the historical period. *Geophysical Research Letters*, 43, 3911– 3920.  
 1133 <https://doi.org/10.1002/2016GL068406>
- 1134 Gregory, J. M., Andrews, T., & Good, P. (2015). The inconstancy of the transient climate response  
 1135 parameter under increasing CO<sub>2</sub>. *Philosophical Transactions of the Royal Society A*, 373, 140– 417.  
 1136 <http://doi.org/10.1098/rsta.2014.0417>
- 1137 Gregory, J. M., Andrews, T., Ceppi, P., Mauritsen, T., & Webb, M. J. (2020). How accurately can the  
 1138 climate sensitivity to CO<sub>2</sub> be estimated from historical climate change? *Climate Dynamics*, 54(1–2),  
 1139 129– 157. <https://doi.org/10.1007/s00382-019-04991-y>
- 1140 Gregory, J. M., Stouffer, R. J., Raper, S. C. B., Stott, P. A., & Rayner, N. A. (2002). An observationally  
 1141 based estimate of the climate sensitivity. *Journal of Climate*, 15(22), 3117– 3121.  
 1142 [https://doi.org/10.1175/1520-0442\(2002\)015<3117:AObEOT>2.0.CO;2](https://doi.org/10.1175/1520-0442(2002)015<3117:AObEOT>2.0.CO;2)
- 1143 Gregory, J. M., et al. (2004). A new method for diagnosing radiative forcing and climate sensitivity.  
 1144 *Geophysical Research Letters*, 31, L03205. <https://doi.org/10.1029/2003GL018747>
- 1145 Hartmann, D. L., and Coauthors, 2013: Observations: Atmosphere and surface. *Climate Change 2013:*  
 1146 *The Physical Science Basis*, T. F. Stocker et al., Eds., Cambridge University Press, 159–254.
- 1147 Hansen, J., Sato, M. K. I., Ruedy, R., Nazarenko, L., Lacis, A., Schmidt, G. A., Russell, G., Aleinov, I.,  
 1148 Bauer, M., Bauer, S. & Bell, N. (2005). Efficacy of climate forcings, mathematical physical and  
 1149 engineering sciences 365, 1925–54. *Journal of Geophysical Research*, 110, D18104.  
 1150 <https://doi.org/10.1029/2005JD005776>

1151 Heede, U.K., Fedorov, A.V. Eastern equatorial Pacific warming delayed by aerosols and thermostat  
1152 response to CO<sub>2</sub> increase. *Nat. Clim. Chang.* **11**, 696–703 (2021). [https://doi.org/10.1038/s41558-](https://doi.org/10.1038/s41558-021-01101-x)  
1153 [021-01101-x](https://doi.org/10.1038/s41558-021-01101-x)

1154 Held, I. M., Guo, H., Adcroft, A., Dunne, J. P., Horowitz, L. W., Krasting, J., et al. (2019). Structure and  
1155 performance of GFDL's CM4.0 climate model. *Journal of Advances in Modeling Earth Systems*, **11**,  
1156 3691– 3727. <https://doi.org/10.1029/2019MS001829>

1157 Held, I. M., Winton, M., Takahashi, K., Delworth, T., Zeng, F., & Vallis, G. K. (2010). Probing the fast  
1158 and slow components of global warming by returning abruptly to preindustrial forcing. *Journal of*  
1159 *Climate*, **23**(9), 2418– 2427. <https://doi.org/10.1175/2009JCLI3466.1>

1160 Hedemann, C., Mauritsen, T., Jungclaus, J. *et al.* The subtle origins of surface-warming hiatuses.  
1161 *Nature Clim Change* **7**, 336–339 (2017). <https://doi.org/10.1038/nclimate3274>

1162 Hurrell, J., Hack, J., Shea, D., Caron, J., & Rosinski, J. (2008). A new sea surface temperature and sea  
1163 ice boundary dataset for the community atmosphere model. *Journal of Climate*, **21**(19), 5145– 5153.  
1164 <https://doi.org/10.1175/2008JCLI2292.1>

1165 Hwang, Y.-T., Xie, S.-P., Deser, C., and Kang, S. M. (2017), Connecting tropical climate change with  
1166 Southern Ocean heat uptake, *Geophys. Res. Lett.*, **44**, 9449– 9457, doi:[10.1002/2017GL074972](https://doi.org/10.1002/2017GL074972).

1167 Jiménez-de-la-Cuesta, D., & Mauritsen, T. (2019). Emergent constraints on Earth's transient and  
1168 equilibrium response to doubled CO<sub>2</sub> from post–1970s global warming. *Nature Geoscience*, **12**, 902–  
1169 905. <https://doi.org/10.1038/s41561-019-0463-y>

1170 Kawai, H., S. Yukimoto, T. Koshiro, N. Oshima, T. Tanaka, H. Yoshimura, and R. Nagasawa, 2019:  
1171 Significant Improvement of Cloud Representation in Global Climate Model MRI-ESM2. *Geosci. Model*  
1172 *Dev.*, **12**, 2875-2897.

1173 Lewis, N., & Mauritsen, T. (2021). Negligible Unforced Historical Pattern Effect on Climate Feedback  
1174 Strength Found in HadISST-Based AMIP Simulations, *Journal of Climate*, **34**(1), 39-55.  
1175 <https://doi.org/10.1175/JCLI-D-19-0941.1>.

1176 Lewis, N., & Curry, J. A. (2018). The impact of recent forcing and ocean heat uptake data on  
1177 estimates of climate sensitivity. *Journal of Climate*, **31**, 6051– 6071.

1178 Li, C., von Storch, J.-S., & Marotzke, J. (2013). Deep-ocean heat uptake and equilibrium climate  
1179 response. *Climate Dynamics*, **40**, 1071– 1086.

1180 Liu, C., Allan, R. P., Berrisford, P., Mayer, M., Hyder, P., Loeb, N., Smith, D., Vidale, P.-L., and  
1181 Edwards, J. M. (2015), Combining satellite observations and reanalysis energy transports to estimate  
1182 global net surface energy fluxes 1985–2012, *J. Geophys. Res. Atmos.*, **120**, 9374– 9389,  
1183 doi:[10.1002/2015JD023264](https://doi.org/10.1002/2015JD023264).

1184 Liu, C., Allan, R. P., Mayer, M., Hyder, P., Loeb, N. G., Roberts, C. D., Valdivieso, M., Edwards, J. M.,  
1185 and Vidale, P.-L. (2017), Evaluation of satellite and reanalysis-based global net surface energy flux  
1186 and uncertainty estimates, *J. Geophys. Res. Atmos.*, **122**, 6250– 6272, doi:[10.1002/2017JD026616](https://doi.org/10.1002/2017JD026616).

1187 Liu, C., Allan, R.P., Mayer, M. *et al.* Variability in the global energy budget and transports 1985–2017.  
1188 *Clim Dyn* **55**, 3381–3396 (2020). <https://doi.org/10.1007/s00382-020-05451-8>

1189 Liu, C. and R. Allan (2022): Reconstructions of the radiation fluxes at the top of atmosphere and net  
1190 surface energy flux: DEEP-C Version 5.0. University of Reading. Dataset.  
1191 <https://doi.org/10.17864/1947.000347>.

1192 Loeb, N. G., Johnson, G. C., Thorsen, T. J., Lyman, J. M., Rose, F. G., & Kato, S. (2021). Satellite and  
1193 ocean data reveal marked increase in Earth's heating rate. *Geophysical Research Letters*, 48,  
1194 e2021GL093047. <https://doi.org/10.1029/2021GL093047>.

1195 Loeb, N. G., Wang, H., Allan, R., Andrews, T., Armour, K., Cole, J. N. S., et al. (2020). New generation  
1196 of climate models track recent unprecedented changes in earth's radiation budget observed by  
1197 CERES. *Geophysical Research Letters*, 47, e2019GL086705. <https://doi.org/10.1029/2019GL086705>.

1198 Mauritsen, T., Bader, J., Becker, T., Behrens, J., Bittner, M., Brokopf, R., et al. (2019). Developments  
1199 in the MPI-M Earth System Model version 1.2 (MPI-ESM1.2) and its response to increasing CO<sub>2</sub>.  
1200 *Journal of Advances in Modeling Earth Systems*, 11, 998– 1038.  
1201 <https://doi.org/10.1029/2018MS001400>

1202 Marvel, K., Pincus, R., Schmidt, G. A., & Miller, R. L. (2018). Internal variability and disequilibrium  
1203 confound estimates of climate sensitivity from observations. *Geophysical Research Letters*, 45,  
1204 1595– 1601. <https://doi.org/10.1002/2017GL076468>

1205 Marvel, K., Schmidt, G. A., Miller, R. L., & Nazarenko, L. (2016). Implications for climate sensitivity  
1206 from the response to individual forcings. *Nature Climate Change*, 6, 386– 389).  
1207 <https://doi.org/10.1038/nclimate2888>.

1208 Martin, G.M., et al., 2011: The HadGEM2 family of Met Office Unified Model climate configurations,  
1209 *Geosci. Model Dev.*, 4, 723–757, <https://doi.org/10.5194/gmd-4-723-2011>, 2011.

1210 McGregor, S., Stuecker, M.F., Kajtar, J.B. et al. Model tropical Atlantic biases underpin diminished  
1211 Pacific decadal variability. *Nature Clim Change* 8, 493–498 (2018). [https://doi.org/10.1038/s41558-](https://doi.org/10.1038/s41558-018-0163-4)  
1212 [018-0163-4](https://doi.org/10.1038/s41558-018-0163-4)

1213 Meehl G A, Senior C A, Eyring V, Flato G, Lamarque J-F, Stouffer R J, Taylor K E and Schlund M,  
1214 (2020), Context for interpreting equilibrium climate sensitivity and transient climate response from  
1215 the CMIP6 Earth system models. *Sci. Adv.* 6, 26, <https://doi.org/10.1126/sciadv.aba1981>.

1216 Morice, C. P., Kennedy, J. J., Rayner, N. A., Winn, J. P., Hogan, E., Killick, R. E., et al. (2021). An  
1217 updated assessment of near-surface temperature change from 1850: the HadCRUT5 data set.  
1218 *Journal of Geophysical Research: Atmospheres*, 126, e2019JD032361.  
1219 <https://doi.org/10.1029/2019JD032361>

1220 Moseid, K. O., Schulz, M., Storelvmo, T., Julsrud, I. R., Olivié, D., Nabat, P., Wild, M., Cole, J. N. S.,  
1221 Takemura, T., Oshima, N., Bauer, S. E., and Gastineau, G.: Bias in CMIP6 models as compared to  
1222 observed regional dimming and brightening, *Atmos. Chem. Phys.*, 20, 16023–16040,  
1223 <https://doi.org/10.5194/acp-20-16023-2020>, 2020.

1224 Neale, R. B., Richter, J., Park, S., Lauritzen, P. H., Vavrus, S. J., Rasch, P. J., & Zhang, M. (2013). The  
1225 Mean Climate of the Community Atmosphere Model (CAM4) in Forced SST and Fully Coupled  
1226 Experiments, *Journal of Climate*, 26(14), 5150-5168. <https://doi.org/10.1175/JCLI-D-12-00236.1>.

1227 Newsom, E., Zanna, L., Khatiwala, S., & Gregory, J. M. (2020). The influence of warming patterns on  
1228 passive ocean heat uptake. *Geophysical Research Letters*, 47, e2020GL088429.  
1229 <https://doi.org/10.1029/2020GL088429>

- 1230 Nijse, F. J. M. M., Cox, P. M., & Williamson, M. S. (2020). An emergent constraint on Transient  
 1231 Climate Response from simulated historical warming in CMIP6 models. *Earth System Dynamics*.  
 1232 <https://doi.org/10.5194/esd-2019-86>.
- 1233 Olonscheck, D., Rugenstein, M., & Marotzke, J. (2020). Broad consistency between observed and  
 1234 simulated trends in sea surface temperature patterns. *Geophysical Research Letters*, 47,  
 1235 e2019GL086773. <https://doi.org/10.1029/2019GL086773>
- 1236 Otto, A., Otto, F. E. L., Boucher, O., Church, J., Hegerl, G., Forster, P. M., Gillett, N. P., Gregory, J.,  
 1237 Johnson, G. C., Knutti, R., Lewis, N., Lohmann, U., Marotzke, J., Myhre, G., Shindell, D., Stevens, B., &  
 1238 Allen, M. R. (2013). Energy budget constraints on climate response. *Nature Geoscience*, 6(6), 415–  
 1239 416. <https://doi.org/10.1038/ngeo1836>
- 1240 Pope, D. V., M. Gallani, R. Rowntree, and A. Stratton (2000), The impact of new physical  
 1241 parameterizations in the Hadley Centre climate model: HadAM3, *Clim. Dyn.*, 16(2–3), 123–146.
- 1242 Power, S., et al., (2021). Decadal climate variability in the tropical Pacific: Characteristics, causes,  
 1243 predictability, and prospects. *Science*. 374. eaay9165. [10.1126/science.aay9165](https://doi.org/10.1126/science.aay9165).
- 1244 Proistosescu, C., & Huybers, P. J. (2017). Slow climate mode reconciles historical and model-based  
 1245 estimates of climate sensitivity. *Science Advances*, 3, 1– 7. <https://doi.org/10.1126/sciadv.1602821>
- 1246 Rayner, N. A., Parker, D. E., Horton, E. B., Folland, C. K., Alexander, L. V., Rowell, D. P., Kent, E. C., and  
 1247 Kaplan, A. (2003), Global analyses of sea surface temperature, sea ice, and night marine air  
 1248 temperature since the late nineteenth century, *J. Geophys. Res.*, 108, 4407,  
 1249 doi:[10.1029/2002JD002670](https://doi.org/10.1029/2002JD002670), D14.
- 1250 Raghuraman, S.P., Paynter, D. & Ramaswamy, V. Anthropogenic forcing and response yield observed  
 1251 positive trend in Earth’s energy imbalance. *Nat Commun* **12**, 4577 (2021).  
 1252 <https://doi.org/10.1038/s41467-021-24544-4>
- 1253 Reynolds, R. W., Rayner, N. A., Smith, T. M., Stokes, D. C., & Wang, W. (2002). An Improved In Situ  
 1254 and Satellite SST Analysis for Climate, *Journal of Climate*, 15(13), 1609-1625.
- 1255 Richardson, T. B., Forster, P. M., Smith, C. J., Maycock, A. C., Wood, T., Andrews, T., et al. (2019).  
 1256 Efficacy of climate forcings in PDRMIP models. *Journal of Geophysical Research: Atmospheres*, 124,  
 1257 12824– 12844. <https://doi.org/10.1029/2019JD030581>
- 1258 Rose, B. E. J., Armour, K. C., Battisti, D. S., Feldl, N., & Koll, D. D. (2014). The dependence of transient  
 1259 climate sensitivity and radiative feedbacks on the spatial pattern of ocean heat uptake. *Geophysical  
 1260 Research Letters*, 41, 1– 8.
- 1261 Rugenstein, M. A. A., Caldiera, K., & Knutti, R. (2016). Dependence of global radiative feedbacks on  
 1262 evolving patterns of surface heat fluxes. *Geophysical Research Letters*, 43, 9877– 9885.  
 1263 <https://doi.org/10.1002/2016GL070907>
- 1264 Rugenstein, M., Bloch-Johnson, J., Gregory, J., Andrews, T., Mauritsen, T., Li, C., et al. (2020).  
 1265 Equilibrium climate sensitivity estimated by equilibrating climate models. *Geophysical Research  
 1266 Letters*, 47, e2019GL083898. <https://doi.org/10.1029/2019GL083898>
- 1267 Rugenstein, M. A. A., & Armour, K. C. (2021). Three flavors of radiative feedbacks and their  
 1268 implications for estimating equilibrium climate sensitivity. *Geophysical Research Letters*, 48,  
 1269 e2021GL092983. <https://doi.org/10.1029/2021GL092983>



1270 Sadai, S., Condrón, A., DeConto, R., & Pollard, D. (2020). Future climate response to Antarctic Ice  
1271 Sheet melt caused by anthropogenic warming. *Science advances*, 6(39), eaaz1169.

1272 Sanderson, B. M., and Knutti, R. (2012), On the interpretation of constrained climate model  
1273 ensembles, *Geophys. Res. Lett.*, 39, L16708, doi:[10.1029/2012GL052665](https://doi.org/10.1029/2012GL052665).

1274 Schneider, A., Flanner, M. & Perket, J. Multidecadal variability in surface albedo feedback across  
1275 CMIP5 models. *Geophys. Res. Lett.* **45**, 1972–1980 (2018).

1276 Seager, R., Cane, M., Henderson, N., Lee, D.-E., Abernathy, R., & Zhang, H. (2019). Strengthening  
1277 tropical Pacific zonal sea surface temperature gradient consistent with rising greenhouse gases.  
1278 *Nature Climate Change*, 9, 517– 522.

1279 Senior, C. A., & Mitchell, J. F. B. (2000). The time dependence of climate sensitivity. *Geophysical*  
1280 *Research Letters*, 27, 2685– 2688. <https://doi.org/10.1029/2000GL011373>

1281 Sherwood, S. C., Webb, M. J., Annan, J. D., Armour, K. C., Forster, P. M., Hargreaves, J. C., et al.  
1282 (2020). An assessment of Earth's climate sensitivity using multiple lines of evidence. *Reviews of*  
1283 *Geophysics*, 58, e2019RG000678. <https://doi.org/10.1029/2019RG000678>.

1284 Silvers, L. G., Paynter, D., & Zhao, M. (2018). The diversity of cloud responses to twentieth century  
1285 sea surface temperatures. *Geophysical Research Letters*, 45, 391– 400.  
1286 <https://doi.org/10.1002/2017GL075583>

1287 Smith, D. M., and Coauthors, 2015: Earth's energy imbalance since 1960 in observations and CMIP5  
1288 models. *Geophys. Res. Lett.*, **42**, 1205–1213, <https://doi.org/10.1002/2014GL062669>.

1289 Stevens, B., Sherwood, S. C., Bony, S., & Webb, M. J. (2016). Prospects for narrowing bounds on  
1290 Earth's equilibrium climate sensitivity. *Earth's Future*, 4, 512– 522.  
1291 <https://doi.org/10.1002/2016EF000376>.

1292 Swart, N. C., Cole, J. N. S., Kharin, V. V., Lazare, M., Scinocca, J. F., Gillett, N. P., Anstey, J., Arora, V.,  
1293 Christian, J. R., Hanna, S., Jiao, Y., Lee, W. G., Majaess, F., Saenko, O. A., Seiler, C., Seinen, C., Shao,  
1294 A., Sigmond, M., Solheim, L., von Salzen, K., Yang, D., and Winter, B.: The Canadian Earth System  
1295 Model version 5 (CanESM5.0.3), *Geosci. Model Dev.*, 12, 4823–4873, [https://doi.org/10.5194/gmd-](https://doi.org/10.5194/gmd-12-4823-2019)  
1296 12-4823-2019, 2019.

1297 Takahashi, C., and M. Watanabe, 2016: Pacific trade winds accelerated by aerosol forcing over the  
1298 past two decades. *Nature Climate Change*, 6, 768-772, doi: 10.1038/nclimate2996.

1299 Tatebe, H., Ogura, T., Nitta, T., Komuro, Y., Ogochi, K., Takemura, T., Sudo, K., Sekiguchi, M., Abe, M.,  
1300 Saito, F., Chikira, M., Watanabe, S., Mori, M., Hirota, N., Kawatani, Y., Mochizuki, T., Yoshimura, K.,  
1301 Takata, K., O'ishi, R., Yamazaki, D., Suzuki, T., Kurogi, M., Kataoka, T., Watanabe, M., and Kimoto, M.:  
1302 Description and basic evaluation of simulated mean state, internal variability, and climate sensitivity  
1303 in MIROC6, *Geosci. Model Dev.*, 12, 2727–2765, <https://doi.org/10.5194/gmd-12-2727-2019>, 2019.

1304 Taylor, K. E., Stouffer, R. J., & Meehl, G. A. (2012). An overview of CMIP5 and the experiment design.  
1305 *Bulletin of the American Meteorological Society*, 93, 485– 498.

1306 Taylor, K. E., Williamson, D., & Zwiers, F. (2000). The sea surface temperature and sea-ice  
1307 concentration boundary conditions for AMIP II simulations, PCMDI Report No. 60, Program for  
1308 Climate Model Diagnosis and Intercomparison, Lawrence Livermore National Laboratory.

1309 Tierney, J. E., Haywood, A. M., Feng, R., Bhattacharya, T., & Otto-Bliesner, B. L. (2019). Pliocene  
1310 warmth consistent with greenhouse gas forcing. *Geophysical Research Letters*, 46, 9136– 9144.  
1311 <https://doi.org/10.1029/2019GL083802>.

1312 Tierney, J. E., Zhu, J., King, J., Malevich, S.B., Hakim, G.J., & Poulsen, C.J. (2020). Global cooling and  
1313 climate sensitivity revisited. <https://doi.org/10.31223/osf.io/me5uj>.

1314 Titchner, H. A., & Rayner, N. A. (2014). The Met Office Hadley Centre sea ice and sea surface  
1315 temperature data set, version 2: 1. Sea ice concentrations. *Journal of Geophysical Research:*  
1316 *Atmospheres*, 119, 2864– 2889. <https://doi.org/10.1002/2013JD020316>

1317 Tokarska, K. B., Stolpe, M. B., Sippel, S., Fischer, E. M., Smith, C. J., Lehner, F., & Knutti, R. (2020).  
1318 Past warming trend constrains future warming in CMIP6 models. *Science Advance*, 6, eaaz9549.  
1319 <https://doi.org/10.1126/sciadv.aaz9549>.

1320 Voldoire, A., Saint-Martin, D., Sénési, S., Decharme, B., Alias, A., Chevallier, M., et al. (2019).  
1321 Evaluation of CMIP6 DECK experiments with CNRM-CM6-1. *Journal of Advances in Modeling Earth*  
1322 *Systems*, 11, 2177– 2213. <https://doi.org/10.1029/2019MS001683>

1323 Watanabe, M., Dufresne, J.L., Kosaka, Y. *et al.* Enhanced warming constrained by past trends in  
1324 equatorial Pacific sea surface temperature gradient. *Nat. Clim. Chang.* **11**, 33–37 (2021).  
1325 <https://doi.org/10.1038/s41558-020-00933-3>

1326 Webb, M. J., Andrews, T., Bodas-Salcedo, A., Bony, S., Bretherton, C. S., Chadwick, R., Chepfer, H.,  
1327 Douville, H., Good, P., Kay, J. E., Klein, S. A., Marchand, R., Medeiros, B., Siebesma, A. P., Skinner, C.  
1328 B., Stevens, B., Tselioudis, G., Tsushima, Y., and Watanabe, M.: The Cloud Feedback Model  
1329 Intercomparison Project (CFMIP) contribution to CMIP6, *Geosci. Model Dev.*, 10, 359–384,  
1330 <https://doi.org/10.5194/gmd-10-359-2017>, 2017.

1331 Williams, K. D., Copsey, D., Blockley, E. W., Bodas-Salcedo, A., Calvert, D., Comer, R., ... Xavier, P. K.  
1332 (2017). The Met Office Global Coupled model 3.0 and 3.1 (GC3.0 and GC3.1) configurations. *Journal*  
1333 *of Advances in Modeling Earth Systems*, 10, 357– 380. <https://doi.org/10.1002/2017MS001115>

1334 Yukimoto, S., H. Kawai, T. Koshiro, N. Oshima, K. Yoshida, S. Urakawa, H. Tsujino, M. Deushi, T.  
1335 Tanaka, M. Hosaka, S. Yabu, H. Yoshimura, E. Shindo, R. Mizuta, A. Obata, Y. Adachi, and M. Ishii,  
1336 2019: The Meteorological Research Institute Earth System Model version 2.0, MRI-ESM2.0:  
1337 Description and basic evaluation of the physical component. *J. Meteor. Soc. Japan*, 97, 931-965.

1338 Zelinka, M. D., Myers, T. A., McCoy, D. T., Po-Chedley, S., Caldwell, P. M., Ceppi, P., Klein, S. A., &  
1339 Taylor, K. E. (2020). Causes of higher climate sensitivity in CMIP6 models. *Geophysical Research*  
1340 *Letters*, 47, e2019GL085782. <https://doi.org/10.1029/2019GL085782>

1341 Zhang, L., Delworth, T.L., Cooke, W. *et al.* Natural variability of Southern Ocean convection as a  
1342 driver of observed climate trends. *Nature Clim Change* **9**, 59–65 (2019).  
1343 <https://doi.org/10.1038/s41558-018-0350-3>

1344 Zhou, C., Zelinka, M. D., & Klein, S. A. (2016). Impact of decadal cloud variations on the Earth's  
1345 energy budget. *Nature Geoscience*, 9, 871– 875.

1346 Zhou, C., Zelinka, M.D., Dessler, A.E. *et al.* Greater committed warming after accounting for the  
1347 pattern effect. *Nat. Clim. Chang.* **11**, 132–136 (2021). <https://doi.org/10.1038/s41558-020-00955-x>

1348 Zhu, J., B.L. Otto-Bliesner, E.C. Brady, C. Poulson, J.K. Shaw, J.E. Kay (2022), LGM paleoclimate  
1349 constraints inform cloud parameterizations and equilibrium climate sensitivity in CESM2. Earth and  
1350 Space Science Open Archive, <https://doi.org/10.1002/essoar.10507790.1>.

1351

1352 **Table1: Summary of the Atmospheric General Circulation Model (AGM) simulations used in this study.** *amip-piForcing* refers to an AGCM simulation  
 1353 forced with time-varying observed monthly SSTs and sea-ice using the AMIP II boundary condition SST and sea-ice dataset, forcing agents such greenhouse  
 1354 gases, aerosol emission etc. are kept at pre-industrial levels. *hadSST-piForcing* is identical in all aspects except SSTs are taken from the HadISST1 database  
 1355 (sea-ice remains the same as *amip-piForcing*). The ensemble size and time-periods covered for each experiment and AGCM is indicated. *amip-piForcing*  
 1356 simulations included in the CFMIP3 (Webb et al. 2017) contribution to CMIP6 are indicated by a y/n. The corresponding name of each AGCMs parent  
 1357 AOGCM is indicated. Global-annual-ensemble-mean dT and dN timeseries data are available for all *amip-piForcing* and *hadSST-piForcing* AGCM simulations  
 1358 (see Data Availability Statement).

AGCM	Corresponding AOGCM name	Model description	<i>amip-piForcing</i>			<i>hadSST-piForcing</i>	
			CMIP6? (y/n)	Ensemble size	Time-period covered	Ensemble size	Time-period covered
<b>CAM4</b>	CCSM4	Neale et al. (2013)	n	3	1870 – 2014	3	1870 – 2014
<b>CESM2</b>	unchanged	Danabasoglu et al. (2020)	y	1	1870 – 2014	-	-
<b>CNRM-CM6-1</b>	unchanged	Voltaire et al. (2019)	y	1	1870 – 2014	-	-
<b>CanESM5</b>	unchanged	Swart et al. (2019)	y	3	1870 – 2014	-	-
<b>ECHAM6.3</b>	MPI-ESM1.1	Mauritsen et al. (2019)	n	5	1871 – 2010	5	1871 – 2015
<b>GFDL-AM3</b>	GFDL-CM3	Donner et al. (2011)	n	1	1870 – 2014	1	1870 – 2014
<b>GFDL-AM4</b>	GFDL-CM4	Held et al. (2019)	n	1	1870 – 2016	1	1870 – 2016
<b>HadAM3</b>	HadCM3	Pope et al. (2000)	n	4	1871 – 2012	4	1871 – 2012
<b>HadGEM2</b>	HadGEM2-ES	Martin et al. (2011)	n	4	1871 – 2012	1	1871 – 2012
<b>HadGEM3-GC31-LL</b>	unchanged	Williams et al. (2017)	y	1	1870 – 2014	1	1871 – 2016
<b>IPSL-CM6A-LR</b>	unchanged	Boucher et al. (2020)	y	1	1870 – 2014	-	-
<b>MIROC6</b>	unchanged	Tatebe et al. (2019)	y	1	1870 – 2014	-	-
<b>MRI-ESM2-0</b>	unchanged	Yukimoto et al. (2019), Kawai et al. (2019)	y	1	1870 – 2014	-	-
<b>MPI-ESM1-2-LR</b>	unchanged	Mauritsen et al. (2019)	n	3	1871 – 2017	3	1871 – 2017

1359

1360

1361 **Table 2: Feedback parameter in *amip-piForcing* and *hadSST-piForcing* simulations over various historical time-periods, as well as *abrupt-4xCO2***  
1362 **sensitivity parameters.**  $\lambda$  values from *amip-piForcing* and *hadSST-piForcing* are calculated from OLS regression ( $\lambda = dN/dT$ ) over the relevant time-periods  
1363 using global-annual-mean timeseries data.  $F_{2xCO_2}$  is calculated as  $F_{4xCO_2}/2$  and  $ECS = -F_{2x}/\lambda_{4xCO_2}$  from 150 years of *abrupt-4xCO2* experiments ( $\lambda_{4xCO_2}$  calculated  
1364 over years 1-20 and 21-150 is also shown) (see Andrews et al., 2012; 2015).

	abrupt-4xCO2					$\lambda_{1871-2010}$ (W m <sup>-2</sup> K <sup>-1</sup> )		$\lambda_{1871-1980}$ (W m <sup>-2</sup> K <sup>-1</sup> )		$\lambda_{1981-2010}$ (W m <sup>-2</sup> K <sup>-1</sup> )	
	ECS (K)	$F_{2x}$ (W m <sup>-2</sup> )	$\lambda_{4xCO_2}$ (W m <sup>-2</sup> K <sup>-1</sup> )	$\lambda_{4xCO_2, 1-20}$ (W m <sup>-2</sup> K <sup>-1</sup> )	$\lambda_{4xCO_2, 21-150}$ (W m <sup>-2</sup> K <sup>-1</sup> )	AMIP	HadISST1	AMIP	HadISST1	AMIP	HadISST1
CAM4	2.95	3.64	-1.23	-1.52	-0.94	-2.14	-1.77	-1.22	-1.45	-2.84	-2.70
CESM2	5.16	3.39	-0.66	-1.17	-0.49	-1.93	-	-0.87	-	-3.08	-
CNRM-CM6-1	4.88	3.66	-0.75	-0.93	-0.87	-1.23	-	-1.10	-	-1.64	-
CanESM5	5.61	3.64	-0.65	-0.70	-0.59	-1.44	-	-0.93	-	-1.83	-
ECHAM6_3	3.01	4.10	-1.36	-1.47	-1.08	-1.92	-1.57	-1.43	-1.38	-2.69	-2.42
GFDL-AM3	3.99	2.97	-0.74	-1.13	-0.61	-1.44	-1.35	-0.72	-0.99	-1.90	-1.41
GFDL-AM4	3.84	3.32	-0.86	-1.54	-0.60	-1.84	-1.66	-1.33	-1.40	-2.57	-2.93
HadAM3	3.37	3.52	-1.04	-1.25	-0.75	-1.65	-1.44	-1.35	-1.40	-2.19	-1.86
HadGEM2	4.62	2.90	-0.63	-0.81	-0.33	-1.39	-1.04	-1.12	-1.08	-2.26	-1.54
HadGEM3-GC31-LL	5.54	3.49	-0.63	-0.81	-0.60	-1.28	-1.01	-0.95	-0.84	-1.87	-1.55
IPSL-CM6A-LR	4.56	3.41	-0.75	-0.98	-0.61	-1.59	-	-1.17	-	-2.50	-
MIROC6	2.58	3.72	-1.44	-1.61	-1.60	-1.42	-	-1.21	-	-1.87	-
MRI-ESM2-0	3.13	3.44	-1.10	-1.68	-0.78	-1.93	-	-1.23	-	-2.79	-
MPI-ESM1-2-LR	3.02	4.21	-1.39	-1.61	-1.34	-1.88	-1.58	-1.30	-1.45	-2.55	-2.42
MEAN	4.02	3.53	-0.95	-1.23	-0.80	-1.65	-1.43	-1.14	-1.25	-2.33	-2.10
1.645 $\sigma$	1.64	0.57	0.49	0.54	0.55	0.46	0.43	0.33	0.37	0.72	0.90

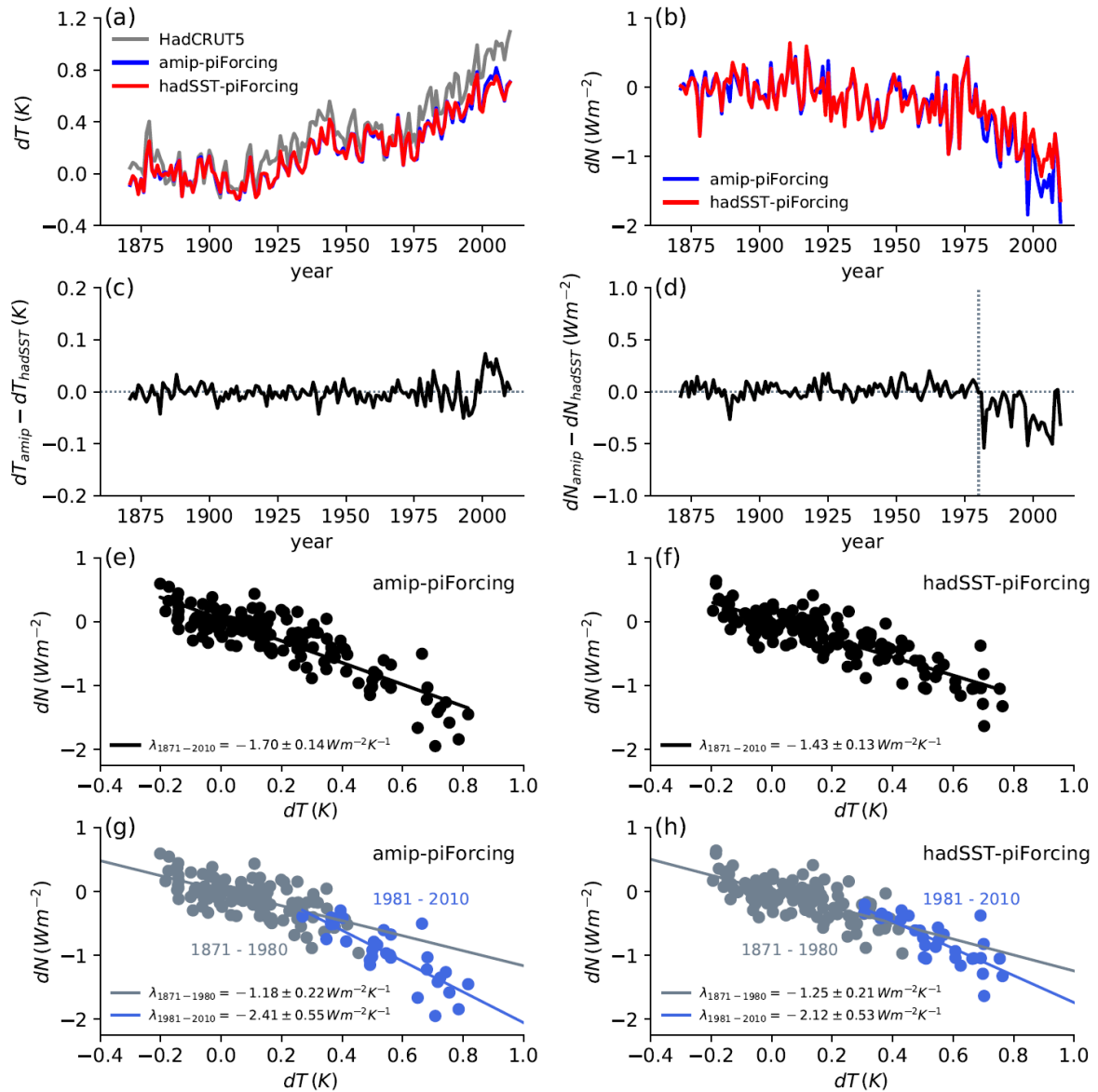
1365 **Table 3: The pattern effect ( $\Delta\lambda = \lambda_{4xCO_2} - \lambda_{hist}$ , with  $\lambda_{4xCO_2}$  from years 1-150 of *abrupt-4xCO2*)**  
1366 **between *abrupt-4xCO2* radiative feedback and radiative feedback calculated over different**  
1367 **historical periods (i.e.  $\lambda_{hist}$  from 1871-2010, and its separation into 1871-1980 and 1981-2010) in**  
1368 ***amip-piForcing* and *hadSST-piForcing*, as well as their difference.**

	1871 – 2010 (W m <sup>-2</sup> K <sup>-1</sup> )			1871 – 1980 (W m <sup>-2</sup> K <sup>-1</sup> )			1981 – 2010 (W m <sup>-2</sup> K <sup>-1</sup> )		
	AMIP	HadSST	Diff	AMIP	HadSST	Diff	AMIP	HadSST	Diff
<b>CAM4</b>	0.90	0.53	0.37	-0.01	0.22	-0.23	1.60	1.47	0.13
<b>CESM2</b>	1.27			0.21			2.43		
<b>CNRM-CM6-1</b>	0.48			0.35			0.89		
<b>CanESM5</b>	0.80			0.28			1.19		
<b>ECHAM6_3</b>	0.56	0.21	0.35	0.07	0.02	0.05	1.32	1.06	0.26
<b>GFDL-AM3</b>	0.69	0.61	0.08	-0.03	0.24	-0.27	1.15	0.67	0.48
<b>GFDL-AM4</b>	0.97	0.80	0.17	0.47	0.53	-0.06	1.70	2.07	-0.37
<b>HadAM3</b>	0.61	0.40	0.21	0.31	0.35	-0.04	1.15	0.82	0.33
<b>HadGEM2</b>	0.76	0.41	0.35	0.49	0.45	0.04	1.63	0.91	0.72
<b>HadGEM3-GC31-LL</b>	0.65	0.38	0.27	0.32	0.21	0.11	1.24	0.92	0.32
<b>IPSL-CM6A-LR</b>	0.84			0.43			1.76		
<b>MIROC6</b>	-0.02			-0.23			0.42		
<b>MRI-ESM2-0</b>	0.83			0.14			1.69		
<b>MPI-ESM1-2-LR</b>	0.49	0.19	0.30	-0.09	0.06	-0.15	1.16	1.03	0.13
<b>MEAN</b>	0.70	0.44	0.26	0.19	0.26	-0.07	1.38	1.12	0.26
<b>1.645<math>\sigma</math></b>	0.47	0.31	0.16	0.35	0.28	0.07	0.75	0.69	0.06

1369

1370 **Table 4: Comparison of the 1985-2014 climate resistance ( $\rho = dF/dT$ ), feedback parameter ( $-\lambda = -$   
1371  $d(N - F)/dT$  and ocean heat uptake efficiency ( $\kappa = dN/dT$ ) using different versions of the DEEP-C  
1372 (Allan et al., 2014) satellite based reconstruction of  $dN$  (see Section 2.4). The lower half of the  
1373 table shows how  $\rho$ ,  $\lambda$  and  $\kappa$  estimates change as the 30 year moving window advances to 1990-  
1374 2019. In all calculations HadCRUT5 analysis  $dT$  (Morice et al. 2021) and IPCC AR6  $dF$  (Forster et al.,  
1375 2021) are used. Years 1991-2 are excluded from the calculation as these years are identified as  
1376 being strongly impacted by the volcanic forcing from the Pinatubo eruption (Section 4).**

<b>dN dataset version</b>	<b>Start year</b>	<b>End year</b>	<b><math>\rho</math> (<math>W m^{-2} K^{-1}</math>)</b>	<b><math>-\lambda</math> (<math>W m^{-2} K^{-1}</math>)</b>	<b><math>\kappa</math> (<math>W m^{-2} K^{-1}</math>)</b>
DEEP-C v2G			2.38	2.24	0.14
DEEP-C v3			2.38	2.24	0.14
DEEP-C v3G	1985	2014	2.38	2.24	0.14
DEEP-C v4			2.38	1.98	0.41
DEEP-C v5			2.38	1.98	0.41
DEEP-C v5	1986	2015	2.38	1.75	0.63
DEEP-C v5	1987	2016	2.25	1.55	0.70
DEEP-C v5	1988	2017	2.21	1.62	0.59
DEEP-C v5	1989	2018	2.23	1.66	0.57
DEEP-C v5	1990	2019	2.30	1.44	0.86



1377

1378

1379

1380

1381

1382

1383

1384

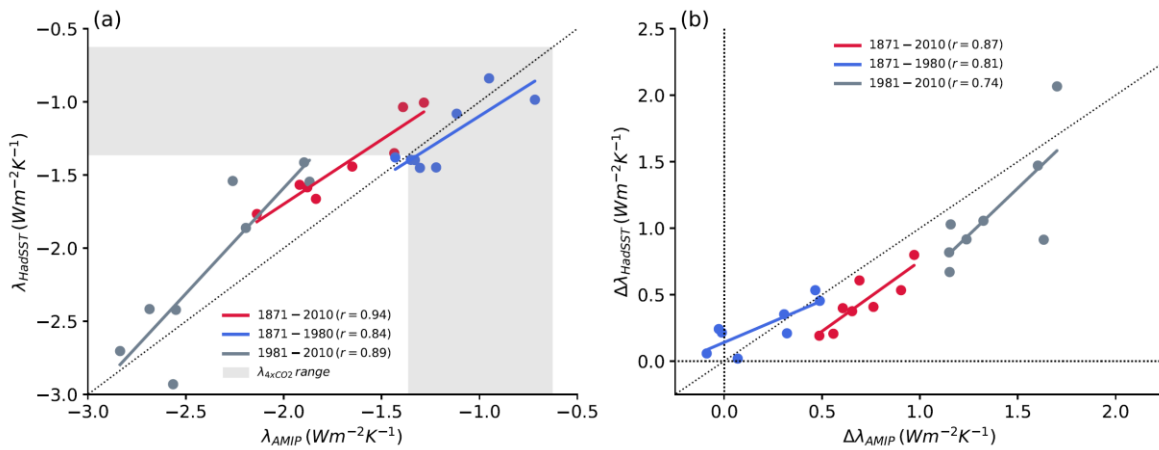
1385

1386

**Figure 1: Comparison of multi-model ensemble-annual-mean (a)  $dT$  and (b)  $dN$  in the *amip-piForcing* and *hadSST-piForcing* simulations. (c) and (d) shows the difference in  $dT$  and  $dN$  respectively, highlighting 1980 as a key year where the  $dN$  response diverges according to the SST dataset. In (a) the HadCRUT5 observed  $dT$  evolution is shown for comparison. (e) and (f) show the relationship between global-annual-mean  $dT$  and  $dN$  in *amip-piForcing* and *hadSST-piForcing* respectively, where  $\lambda=dN/dT$  is calculated from OLS regression on the global-annual-mean data points. The stated 5-95% uncertainty is  $\pm 1.645\sigma$  from the standard error of the linear fit. (g) and (h) show the  $dT$  and  $dN$  relationship separated into two time-periods: years 1871-1980 (grey) and years 1981-2010 (blue).**



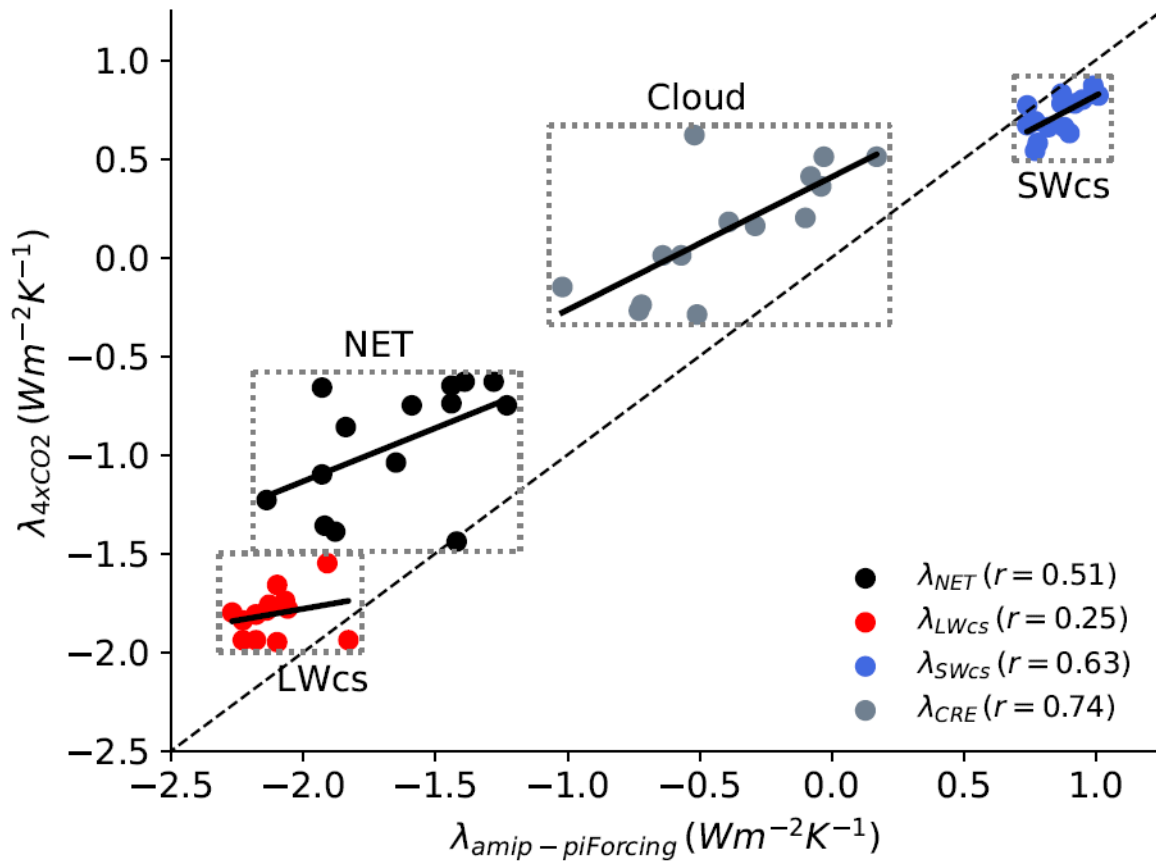
1387



1388

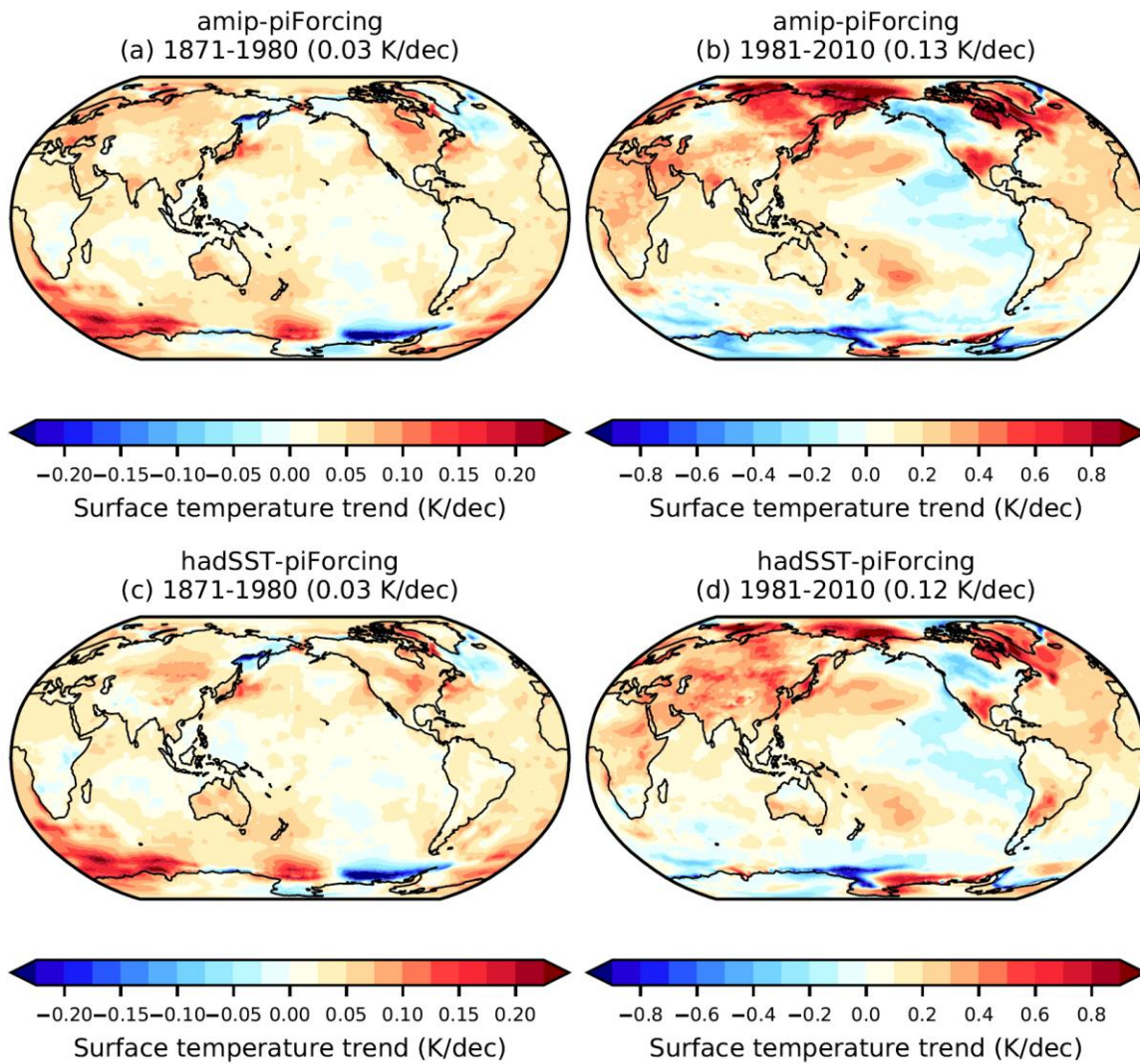
1389 **Figure 2: (a) Relationship between the feedback parameter,  $\lambda$ , in the *amip-piForcing* and *hadSST-***  
1390 ***piForcing* simulations over various historical time-periods. Each point is a single AGCM. The**  
1391 **shaded grey region shows the range of  $\lambda_{4xCO2}$  from the AGCMs corresponding parent AOGCM**  
1392 ***abrupt-4xCO2* simulation. The one-to-one line (dotted) is shown. (b) Relationship between the**  
1393 **pattern effect,  $\Delta\lambda = \lambda_{4xCO2} - \lambda_{hist}$ , diagnosed from the *amip-piForcing* and *hadSST-piForcing***  
1394 **simulations over various historical time-periods.**

1395



1396

1397 **Figure 3: Relationship across models (dots) between the feedback parameter in *amip-piForcing***  
 1398 **(calculated over years 1871-2010) and *abrupt-4xCO2* simulation (calculated over years 1-150). The**  
 1399 **net feedback parameter is decomposed into its longwave clear-sky, SW clear-sky and cloud**  
 1400 **radiative effect components.**



1401

1402

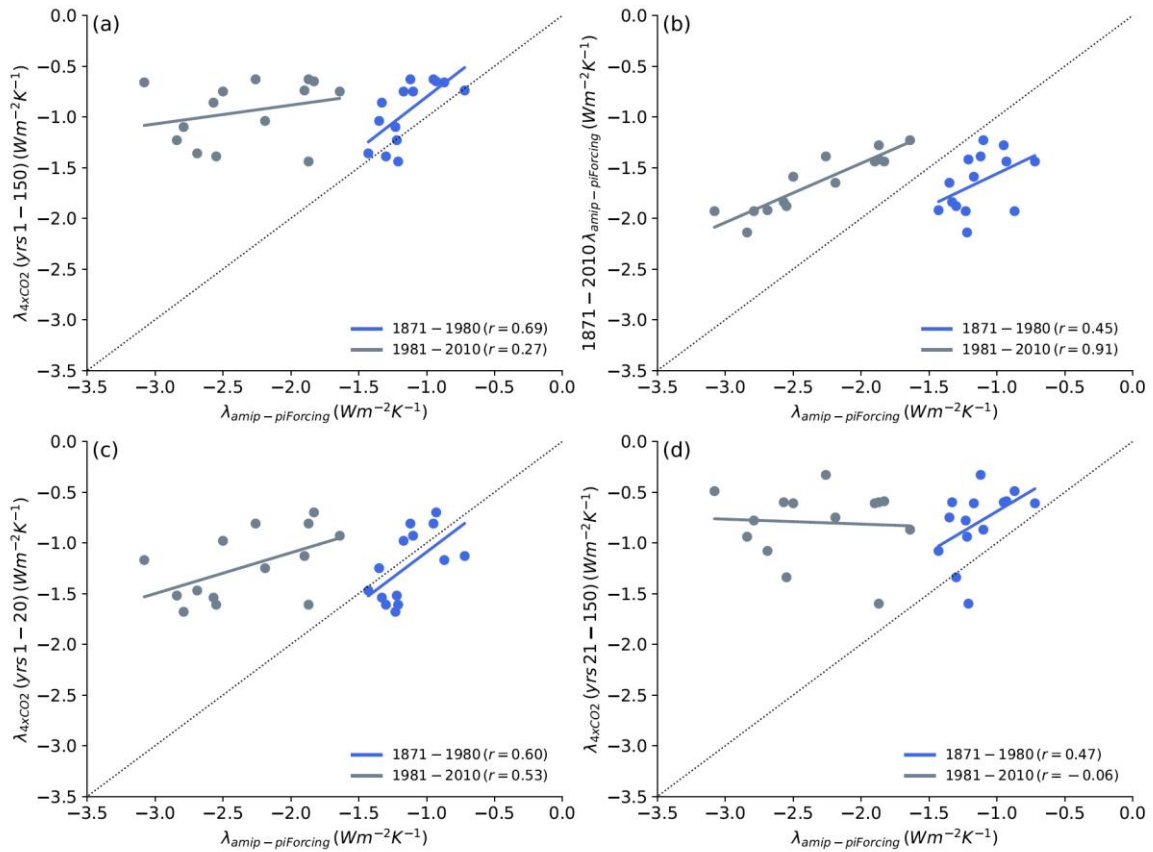
1403

1404

1405

**Figure 4: Decadal surface temperature trends over 1870-1980 and 1981-2010 in (a) and (b) *amip-piForcing* and (c) and (d) *hadSST-piForcing*. Trends are calculated from the linear regression of  $dT$  against time over the corresponding time-periods, on annual-mean data. Data from HadGEM3-GC31-LL simulations have been used for this illustration.**

1406



1407

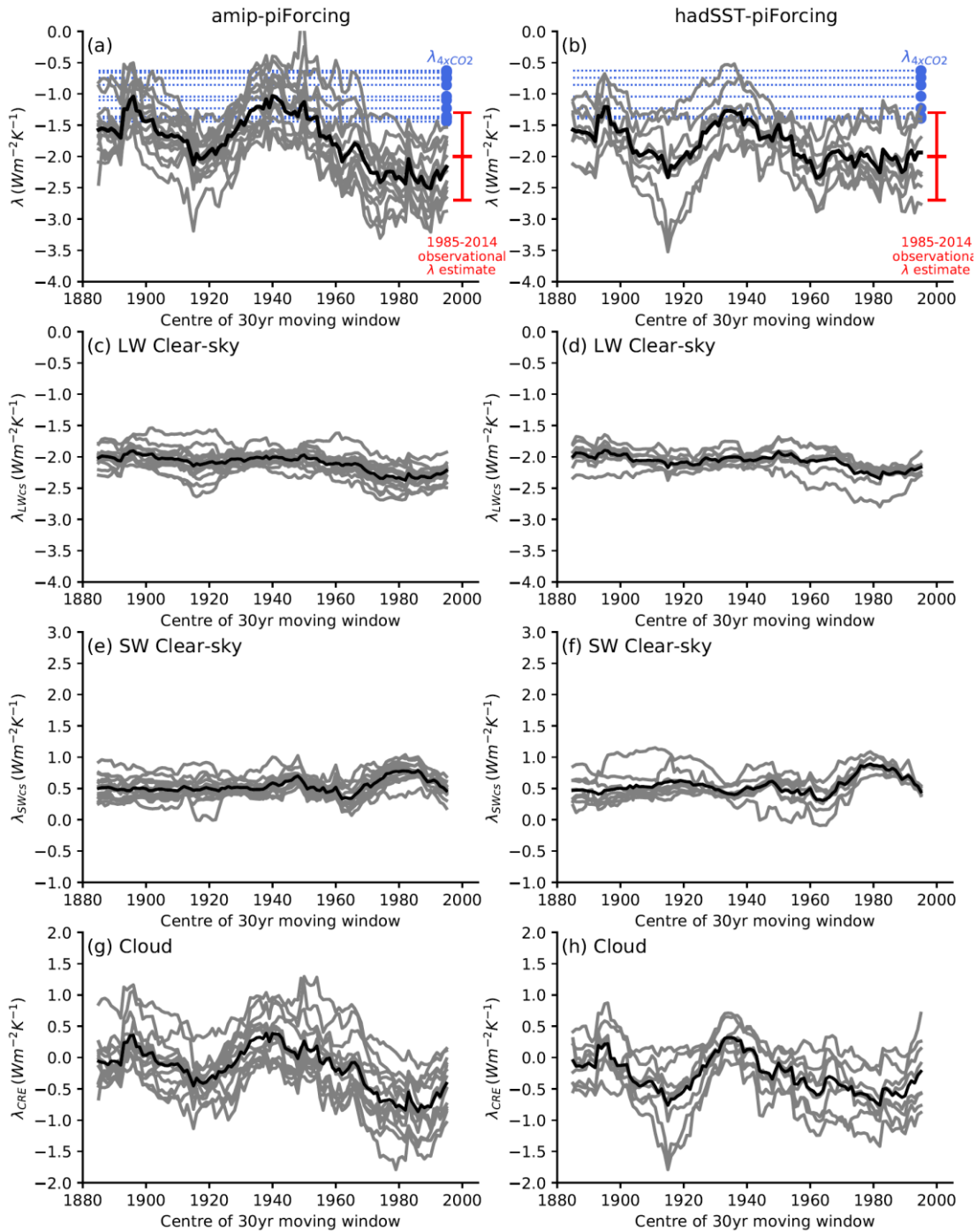
1408

1409

1410

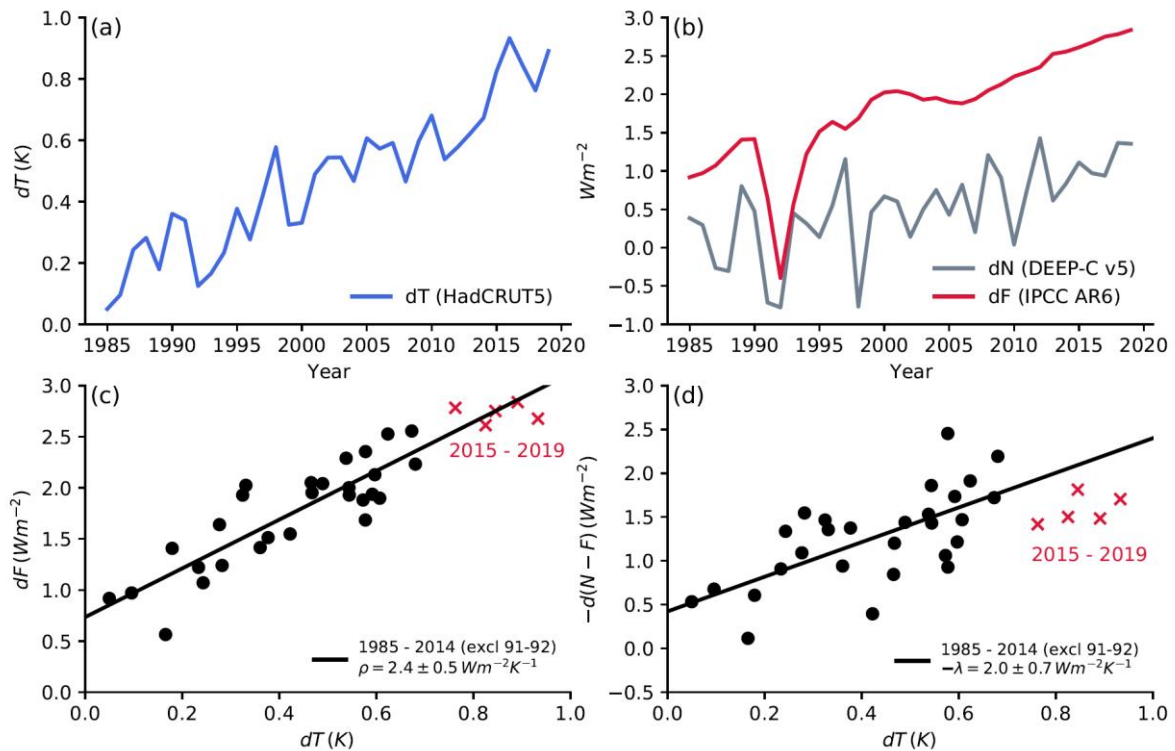
1411

**Figure 5: Relationships between model simulated feedbacks in  $amip-piForcing$  over years 1871-1980 (blue) or 1981-2010 (grey) and (a)  $\lambda_{4xCO2}$  from *abrupt-4xCO2*, (b)  $\lambda_{hist}$  over the entire historical record (1871-2010), (c)  $\lambda_{4xCO2}$  from *abrupt-4xCO2* over years 1-20 and (d) years 21-150.**



1412

1413 **Figure 6: Decadal variation in the feedback parameter  $\lambda$  from 1871 to 2010. Left column shows**  
 1414 **results from *amip-piForcing* and right column shows results from *hadSST-piForcing*. Each grey line**  
 1415 **represents a single AGCM (see Table 1). Thick black is the ensemble-mean of the results. X-axis**  
 1416 **represents the centre of a 30 year moving window in which  $\lambda=dN/dT$  is calculated from OLS**  
 1417 **regression on annual-mean data, i.e.  $\lambda$  at 1980.5 represents the feedback parameter over years**  
 1418 **1966 to 1995. Shown in (a) and (b) is the net feedback parameter. Blue dots and lines represent**  
 1419 **the corresponding  $\lambda_{4xCO2}$  values from AOGCM *abrupt-4xCO2* simulations (Table 2). Red shows an**  
 1420 **observational estimate and 5-95% uncertainty of  $\lambda=d(N - F)/dT \sim -2.0 \pm 0.7 \text{ W m}^{-2} \text{ K}^{-1}$  over years**  
 1421 **1985-2014 (see Section 4). (c) – (h) shows the corresponding LW clear-sky, SW clear-sky and cloud**  
 1422 **radiative effect (CRE) components of  $\lambda$ .**

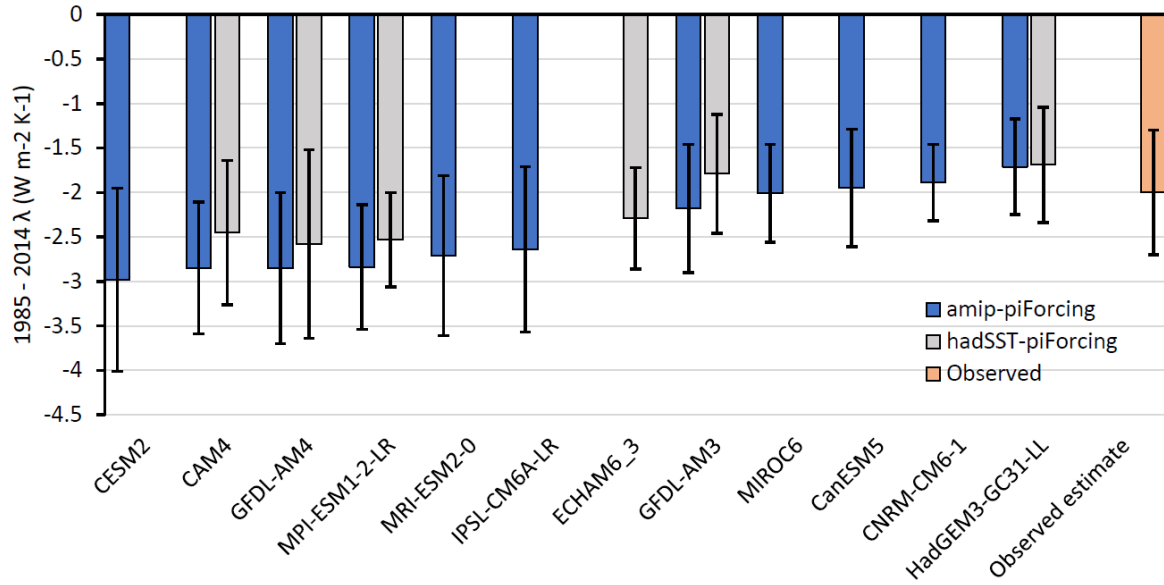


1423

1424 **Figure 7: Observational estimate of the Earth's 1985-2019 energy balance. All points are global-**  
 1425 **annual-means. (a)  $dT$  (HadCRUT5 analysis dataset; Morice et al., 2021), (b)  $dN$  (DEEP-C v5; Allan et**  
 1426 **al., 2014; Liu and Allan, 2022) and  $dF$  (IPCC AR6; Forster et al., 2021). (c)  $\rho = dF/dT$  relationship and**  
 1427 **(d)  $-\lambda_{\text{hist}} = -d(N - F)/dT$  relationship over years 1985-2014. Black dots are global-annual means over**  
 1428 **years 1985-2014 excluding years 1991-2 which are strongly influenced by the Pinatubo explosive**  
 1429 **volcanic eruption (see red line panel b). Red points in (c) and (d) are years 2015-2019. The stated**  
 1430 **5-95% uncertainties are  $\pm 1.645\sigma$  from the standard error of the linear fit.**

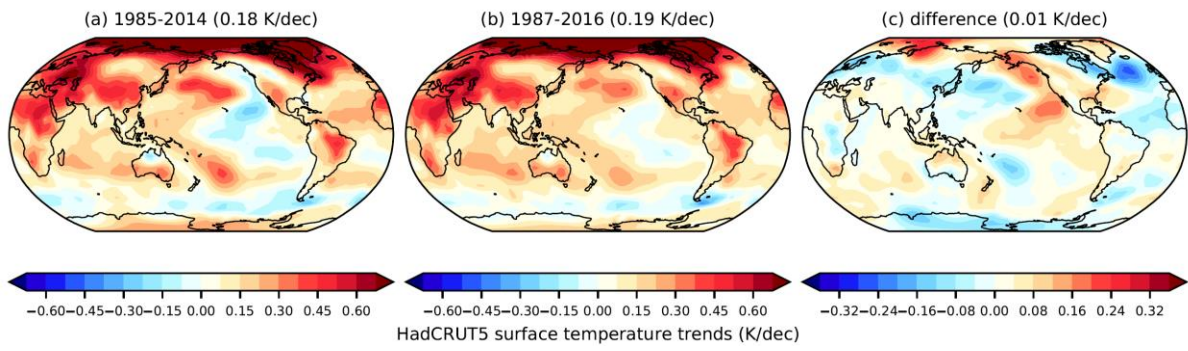
1431

1432



1433

1434 **Figure 8: Comparison of the 1985-2014 feedback parameter,  $\lambda_{\text{hist}} = d(N - F)/dT$ , in *amip-piForcing***  
 1435 **and *hadSST-piForcing* simulations to an observed estimate based on DEEP-C V5  $dN$  (Allan et al.,**  
 1436 **2014; Liu and Allan, 2022), HadCRUT5 analysis  $dT$  (Morice et al. 2021) and IPCC AR6  $dF$  (Forster et**  
 1437 **al., 2021). The 5-95% uncertainty is simply  $1.645\sigma$  from the standard error of the linear fit, with no**  
 1438 **allowance for systematic uncertainties. Note also that years 1991-2 are excluded from the**  
 1439 **calculation as these years are identified as being strongly impacted by the volcanic forcing from**  
 1440 **the Pinatubo eruption (Figure 7b).**



1441

1442 **Figure 9: Decadal trend in near-surface temperature change over (a) 1985-2014 and (b) 1987-2016,**  
 1443 **(c) shows the difference (b minus a). Data is the HadCRUT5 analysis dataset (Morice et al. 2021).**

1444 **Trends are calculated from linear regression on annual-mean data points at each grid box.**